AD NUMBER

AD872033

NEW LIMITATION CHANGE

TO

Approved for public release, distribution unlimited

FROM

Distribution authorized to U.S. Gov't. agencies and their contractors; Administrative/Operational use; Aug 1969. Other requests shall be referred to Army Missile Command, Redstone Arsenal, AL 35898.

AUTHORITY

USAMICOM ltr 7 dec 197272

REPORT NO. RD-TN-69-7

DETAILED ANALYSES FOR THE BASE-PRESSURE PROGRAMS (TSABPP- 1,2)

by

A. L. Addy

Contract No.
DA-01-021-AMC-13902(Z)
University of Illinois
605 S. Goodwin Avenue
Urbana, Illinois 61803

August 1969

U.S. ARMY MISSILE COMMAND
Redstone Arsenal, Alabama 35809

25 August 1969 Report No. RD-TN-69-7

DETAILED ANALYSES FOR THE BASE-PRESSURE PROGRAMS (TSABPP- 1,2)

by

A. L. Addy

Contract No.
DA-01-021-AMC-13902(Z)
University of Illinois
605 S. Goodwin Avenue
Urbana, Illinois 61803

DA Project No. 1M262301A206
AMC Management Structure Code No. 522C.11.148

Aeı dynamics Branch
Advance l Systems Laboratory
Research and Engineering Directorate (Provisional)
U. S. Army Missile Command
Redstone Arsenal, Alabama 35809

ABSTRACT

The detailed development of the analyses which are the bases for the two-stream axisymmetric base-pressure programs (TSABPP-1,2) is presented. For the "corresponding" inviscid flow field, these analyses include the Prandtl-Meyer expansion, the oblique shock wave, the slip line, and the method of characteristics. For the turbulent-mixing component, two-dimensional constant-pressure mixing and its application to axisymmetric flows are considered.

CONTENTS

		Page
1.	Introduction	1
2.	Discussion	1
Appendix A.	MISCELLANEOUS GAS DYNAMICS FUNCTIONS	3
Appendix B.	METHOD OF CHARACTERISTICS	13
Appendix C.	MIXING ANALYSIS: TWO-DIMENSIONAL CONSTANT-PRESSURE TURBULENT MIXING	37
Appendix D.	MIXING ANALYSIS: APPLICATION OF THE TWO-DIMENSIONAL MIXING ANALYSIS TO THE TWO-STREAM AXISYMMETRIC BASE-PRESSURE PROBLEM	51
REFERENCES		61

ILLUSTRATIONS

Table		Page
B-I	Equations of Afterbody Meridional-Plane Profiles	34
B-II	Constants in Afterbody Profile Equations	35
B-III	Expressions for $[x_3, R_3, \theta_3]$ from the Simultaneous Solution of Equations (B-37) and (B-40) for Various Afterbody Shapes	36

Figure		
A-1	Prandtl-Meyer Expansion Notation	4
A-2	Solution Procedure for a Prandtl-Meyer Expansion	5
A-3	Oblique Shock-Wave Notation	6
A-4	Slip Line Flow-Field Configuration	9
A-5	Pressure Turning Angle Configuration for Slip Line Problem	9
A-6	Solution Examples	10
A-7	No-Solution Examples	11
B-1	Physcial Characteristic Curves	14
B-2	General Field Point	15
B-3	Axis Points	19

ILLUSTRATIONS (Concluded)

Figure		Page
B-4	Constant-Pressure Boundary Point	20
B-5	Solid-Boundary Point	22
B-6	Flow-Field Analysis	25
B-7	External Flow-Field Analysis	26
B-8	Same-Family Wave Coalescence	27
B-9	Modification of the Calculation Sequence for Treating Wave Coalescence	27
B-10	Uniform Supersonic Flow Nozzle	29
B-11	Conical Supersonic Flow Nozzle	29
B-12	Characteristics Network for Numerical Calculation of the Initial II-Characteristics for a Conical Nozzle	30
B-13	Approximate Analysis of a Compression at the Nozzle Exit	31
B-14	Initial II-Characteristics for Uniform External Supersonic Flow	32
B-15	Determination of the Final II-Characteristic through the Afterbody Terminus	33
B-16	General Afterbody Notation	34
C-1	Two-Dimensional Mixing Region Control Volume	37
D-1	Approximate Two-Stream Flow Model	51
D-2	Ideal Nozzles and Their Notation	54

1. INTRODUCTION

The purpose of thi : report is to present the detailed development of the principal relationships ai solution techniques which are the bases for the two-stream axisymmetric base-pressure programs (TSABPP-1, 2). While the intent here is to inform the interested program user about these specific programs, it should also be noted that various subsections of these programs are more general, and as such, can serve as basic building blocks in the analysis of other problems. Although an attempt has been made to make this report complete in itself, it is intended and should be considered as supplemental to the technical reports [1, 2] documenting the computer programs.

A uniform notation has been maintained through the reports and the computer programs; since comprehensive lists of symbols are included in the above-referenced technical reports, they are not repeated here.

2. DISCUSSION

In the development of the base-pressure programs, the analyses and the resulting programs were subdivided into three major parts. The first part was the calculation of the "corresponding" inviscid flow field; the second part was the calculation of the mixing component; and the third part was the overall organization of the former calculation sequences into a master program for determining by iteration the base-pressure and base-temperature solutions. This note is not concerned with the latter part, since it is discussed in detail in [1], but rather with the former parts.

The inviscid flow-field analysis consists of the calculation of the supersonic external (free stream) and the internal (nozzle) flows by the method of characteristics. The external flow is over a solid afterbody followed by a constant-pressure boundary region. The internal flow is assumed to be from either an ideal conical or uniform flow nozzle discharging into a region at constant pressure. The supersonic external and internal flows interact at their impingement point, if it exists, to form an oblique shock system and a slip line. The component flow-field analyses are discussed in Appendixes A and B.

The mass entrainment and energy transport rates, due to the turbulent mixing regions formed between the fluid in the wake region and the internal and external streams, are estimated by locally superimposing the two-dimensional constant-pressure turbulent-mixing model at the impingement point of the "corresponding" inviscid streams. The mixing analysis and the "corresponding" inviscid flow-field analyses are then related by the recompression criteria and the requirement of conservation of mass and energy in the wake region. These analyses are discussed in Appendixes C and D.

Appendix A

MISCELLANEOUS GAS DYNAMICS FUNCTIONS

1. Prandtl-Meyer Expansion (EMSPM)

The flow properties before and after a centered Prandtl-Meyer expansion (Figure A-1) are related through the following expression [3]:

$$\omega\left(M_2^*,\ M_{max}^*\right) = \omega\left(M_1^*,\ M_{max}^*\right) + \delta \tag{A-1}$$

where the turning angle, δ, is defined as

$$\delta = \mp(\theta_2 - \theta_1) \tag{A-2}$$

for left- or right-running waves. The $\omega\left(M^*, M_{max}^*\right)$ function is defined by

$$\omega\left(M^*, M_{max}^*\right) = M_{max}^* \tan^{-1}\left\{\left[\frac{M^{*2} - 1}{M_{max}^{*2} - M^{*2}}\right]^{1/2}\right\} - \tan^{-1}\left\{M_{max}^{*2}\left[\frac{M^{*2} - 1}{M_{max}^{*2} - M^{*2}}\right]^{1/2}\right\} \tag{A-3}$$

where $\left(\text{corresponding to } M \to \infty,\ M^* \to M_{max}^*\right)$,

$$M_{max}^* = \left[(\gamma + 1)/(\gamma - 1)\right]^{1/2} . \tag{A-4}$$

The usual problem to be solved is with values of $[M_1^*, \delta, \gamma]$ specified, to find from equations (A-1) and (A-3) the solution value of M_2^*. The numerical solution of these equations can be easily and quickly accomplished as follows.

For expansions, the value of $\omega\left(M_2^*, M_{max}^*\right)$ must be in the range

$$\omega\left(M_1^*, M_{max}^*\right) \le \omega\left(M_2^*, M_{max}^*\right) \le \frac{\pi}{2}\left[M_{max}^* - 1\right] \tag{A-5}$$

and correspondingly, the solution value of M_2^* must be initially in the range

$$M_1^* \le M_2^* \le M_{max}^* . \tag{A-6}$$

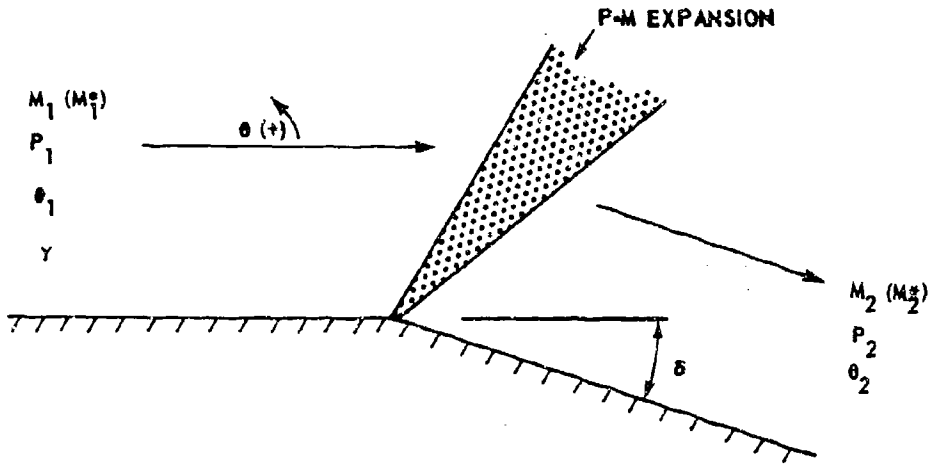

FIGURE A-1. PRANDTL-MEYER EXPANSION NOTATION

For small turning angles, oblique shock waves can be approximated by "reversible compressions"; the initial solution range for those cases is:

$$0 \leq \omega\left(M_2^*, M_{max}^*\right) \leq \omega\left(M_1^*, M_{max}^*\right) \tag{A-7}$$

and

$$1 \leq M_2^* \leq M_1^* \quad . \tag{A-8}$$

For either an expansion or an admissible "reversible compression," rapid convergence to the solution value of M_2^* is achieved by a process of interval halving and, at the same time, successive reduction of the possible solution interval. The solution is always bounded on the negative or positive side relative to the sign of the difference

$$\left[\omega^{(n)}\left(M^{*(n)}, M_{max}^*\right) - \omega\left(M_2^*, M_{max}^*\right)\right] = d^{(n)}$$

If $d^{(n)} < 0$, $M_N^{*(n-1)}$ is replaced by $M^{*(n)}$ and $M_P^{*(n-1)} = M_P^{*(n)}$. On the other hand, if $d^{(n)} > 0$, $M_P^{*(n-1)}$ is replaced by $M^{*(n)}$ and $M_N^{*(n-1)} = M_N^{*(n)}$. This process is continued until the solution is isolated within a calculated interval; i.e., the sign of $d^{(n)}$ has changed at least once. Convergence to the final

solution is then achieved by interpolation and a continuing reduction of the solution interval as before; the solution procedure is illustrated for an expansion in Figure A-2.

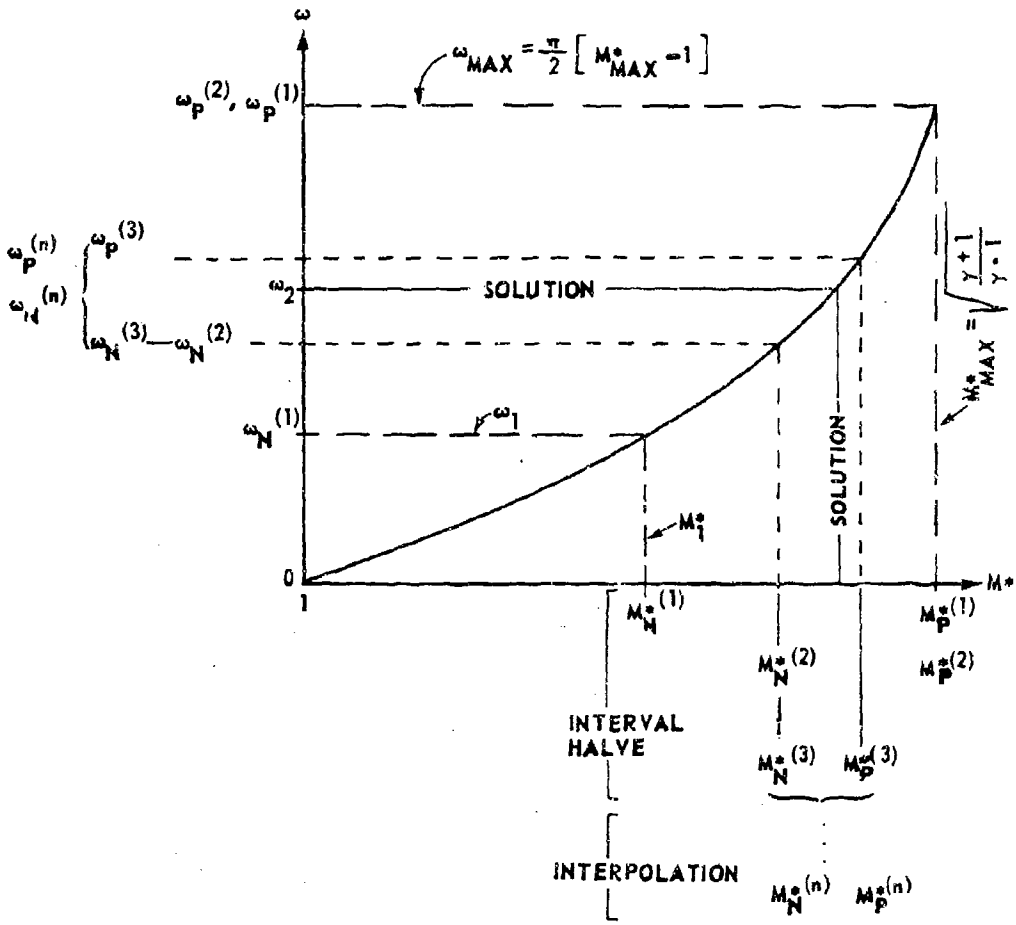

FIGURE A-2. SOLUTION PROCEDURE FOR A PRANDTL-MEYER EXPANSION

The solution criteria are specified as

$$\left| d^{(n)} \Big/ \omega\left(M_2^*, M^*_{max}\right) \right| < \epsilon_1 \dagger$$

and/or

---

† Typically for $\epsilon_1 = \epsilon_2 = 10^{-4}$, $4 < n < 6$ iterations are required.

$$\left| \left[M_P^{*(n)} - M_N^{*(n)} \right] \Big/ M_N^{*(n)} \right| < \epsilon_2 \dagger ,$$

where $d^{(n)}$ is the current value of the difference function and $\left[M_N^{*(n)}, M_P^{*(n)} \right]$ are the current bounds on the solution M_2^*.

2. Oblique Shock Wave (PRSHK)

The general flow situation and notation associated with the analysis of an oblique shock wave are shown in Figure A-3. The expression relating the

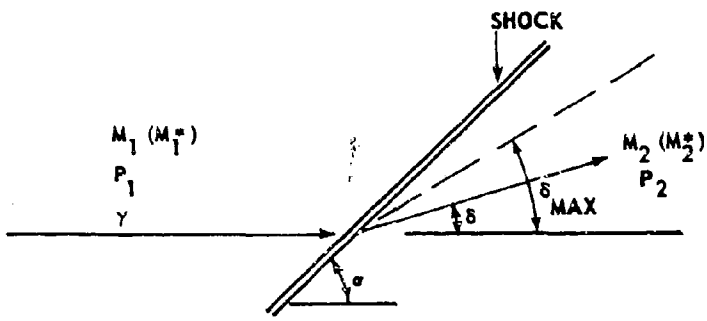

FIGURE A-3. OBLIQUE SHOCK-WAVE NOTATION

oblique shock-wave angle (σ), the approach Mach number (M_1), the turning angle (δ), and the specific heat ratio of the gas (γ) is given [4] as:

$$(\sin^2 \sigma)^3 + b(\sin^2 \sigma)^2 + c(\sin^2 \sigma) + d = 0 \qquad \text{(A-9)}$$

where

$$b = -\left[\frac{M_1^2 + 2}{M_1^2} + \gamma \sin^2 \delta \right] \qquad \text{(A-10)}$$

---

†Typically for $\epsilon_1 = \epsilon_2 = 10^{-4}$, $4 < n < 6$ iterations are required.

$$c = \left[\frac{2M_1^2 + 1}{M_1^4}\right] + \left[\frac{(\gamma + 1)^2}{4} + \frac{(\gamma - 1)}{M_1^2}\right] \sin^2 \delta \quad . \qquad (A-11)$$

$$d = \frac{-\cos^2 \delta}{M_1^4} \quad . \qquad (A-12)$$

Equation (A-9) is simply a cubic equation in $(\sin^2 \sigma)$ whose solution is known. The solutions to equation (A-9) can be written as [5]:

$$Y(I) = 2\sqrt{\frac{-A}{3}} \cos\left[\frac{\phi}{3} + \frac{2(I - 1)}{3}\pi\right] - \frac{b}{3} \quad , \qquad (A-13)$$

where I = 1, 2, or 3 and the Y(I) are the three roots to the cubic equation for $(\sin^2 \sigma)$. The quantities (ϕ, A) are determined from:

$$A = \frac{1}{3}(3c - b^2) \qquad (A-14)$$

$$B = \frac{1}{27}[2b^3 - 9bc + 27d] \qquad (A-15)$$

$$\phi = \cos^{-1}\left\{[-B/2][-A^3/27]^{-1/2}\right\} \quad . \qquad (A-16)$$

For the values of Y(I) to be real, the values of (A, B) must satisfy the requirements that:

$$A < 0 \qquad (A-17)$$

and

$$[-B/2] \leq [-A^3/27]^{1/2} \quad . \qquad (A-18)$$

If equations (A-16) and (A-17) are satisfied, the three roots, Y(I), will all be real. The smallest root corresponds to a physically impossible process; the next larger root corresponds to a weak oblique shock; and the largest root corresponds to a strong oblique shock.

After the weak-shock solution value of $(\sin^2 \sigma)$ has been found all other pertinent dimensionless ratios for an oblique shock wave can be found [4, equations 128 through 149]. Specifically, the static pressure ratio across the shock is found from:

$$\frac{P_2}{P_1} = \frac{2\gamma M_1^2(\sin^2\sigma) - (\gamma - 1)}{(\gamma + 1)} \quad . \tag{A-19}$$

3. Slip-Line Analysis (SLIP)

For an initial slip line solution range, assuming it exists, it is known that (Figures A-4 and A-5)

$$\theta_2 < \theta_s < \theta_1 \tag{A-20}$$

since

$$\left.\begin{aligned} \delta_1 &= -\left(\theta_1 - \theta_s\right) \\ \delta_2 &= -\left(\theta_2 - \theta_s\right) \end{aligned}\right\} \delta_2 - \delta_1 = (\theta_1 - \theta_2) \quad , \tag{A-21}$$

subtracting equations (A-21), the result is:

$$(\delta_1 - \delta_2) = (\theta_1 - \theta_2) = \text{constant across the shock system.} \tag{A-22}$$

Let $\theta_{1s}^{(1)}$ and $\theta_{2s}^{(1)}$ bound the solution on the right and left, respectively. Initially,

$$\left.\begin{aligned} \theta_{1s}^{(1)} &= \theta_1 \\ \theta_{2s}^{(1)} &= \theta_2 \end{aligned}\right\} \text{since } \theta_2 < \theta_s < \theta_1 \quad . \tag{A-23}$$

The solution range can possibly be narrowed for the $\bar{P}$-θ characteristics (weak solution) as shown in Figure A-5. Following this figure, let

$$\left.\begin{aligned} \theta_{1M} &= \left(\theta_1 - \delta_{1M}\right) \\ \theta_{2M} &= \left(\theta_2 + \delta_{2M}\right) \end{aligned}\right\} \delta_{iM} > 0 \tag{A-24}$$

where δ_{iM} are the maximum turning angles for the given γ_i and M_i^*. Now for the solution range,

$$\left.\begin{aligned} &\text{a) if } \theta_{1M} > \theta_2, \text{ set } \theta_{2s}^{(1)} = \theta_{1M} \\ &\text{and/or} \\ &\text{b) if } \theta_{2M} < \theta_1, \text{ set } \theta_{1s}^{(1)} = \theta_{2M} \quad . \end{aligned}\right\} \tag{A-25}$$

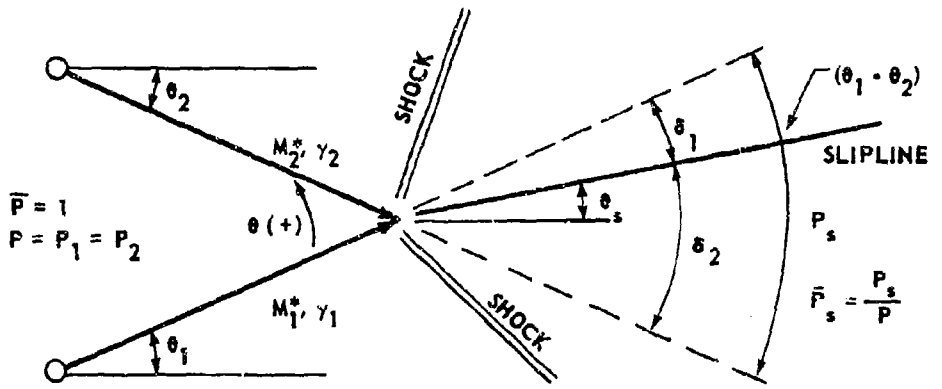

FIGURE A-4. SLIP LINE FLOW-FIELD CONFIGURATION

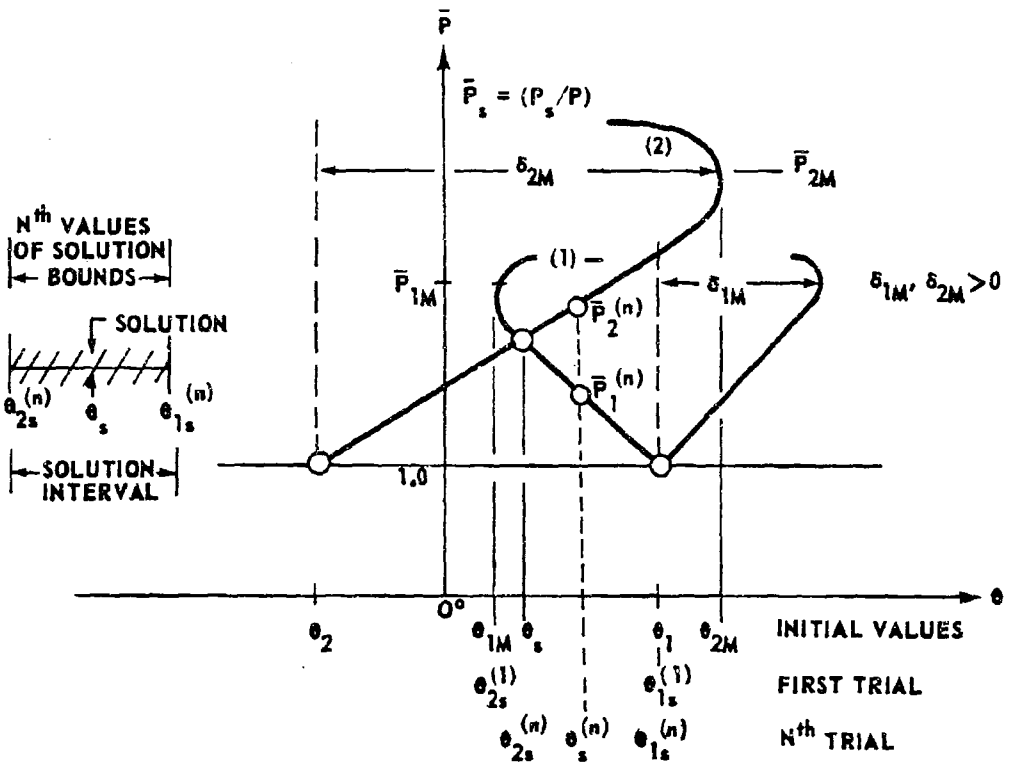

[$\bar{P}$ - θ CURVES (1) AND (2) ARE FOR GIVEN VALUES OF (M_1^*, γ_1) AND (M_2^*, γ_2)]

FIGURE A-5. PRESSURE TURNING ANGLE CONFIGURATION FOR SLIP LINE PROBLEM

Therefore, depending on the magnitudes of θ_1, θ_2, θ_{1M}, θ_{2M}, the solution range is defined by

$$\begin{bmatrix} \theta_{1M} > \theta_2, & \theta_{2s}^{(1)} = \theta_{1M} \\ \text{or} & \\ \theta_{1M} < \theta_2, & \theta_{2s}^{(1)} = \theta_2 \end{bmatrix} < \theta_s < \begin{bmatrix} \theta_{1s}^{(1)} = \theta_1, & \theta_1 < \theta_{2M} \\ \theta_{1s}^{(1)} = \theta_{2M}, & \theta_1 > \theta_{2M} \end{bmatrix} \quad \text{(A-26)}$$

For the possible solution range $\theta_{2s}^{(1)} < \theta_s < \theta_{1s}^{(1)}$, does a solution exist?

If $\left[\bar{P}_{2s}^{(1)} < \bar{P}_{1M} \text{ and } \bar{P}_{1s}^{(1)} < \bar{P}_{2M}\right]$, then a solution must exist in the range $\theta_{2s}^{(1)} < \theta_s < \theta_{1s}^{(1)}$. Cases 1 and 2, Figure A-6, illustrate typical slip-line solutions and the determination of the initial solution range.

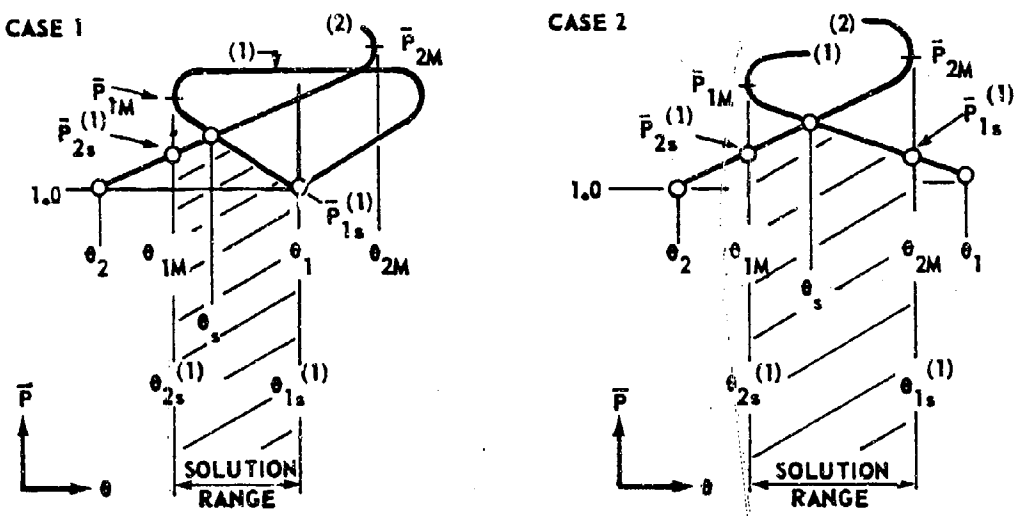

FIGURE A-6. SOLUTION EXAMPLES

If $P_{2s}^{(1)} > P_{1M}$ and/or $P_{1s}^{(1)} > P_{2M}$, no weak solution exists for the given conditions (Case 1, Figure A-7).

If $\theta_{1M} > \theta_{2M}$ → No solution (Case 2, Figure A-7).

If $\theta_{2M} > \theta_{1M}$ → Possible solution; needs further analysis (Cases 1, 2 in Figure A-6 and Case 1 in Figure A-7).

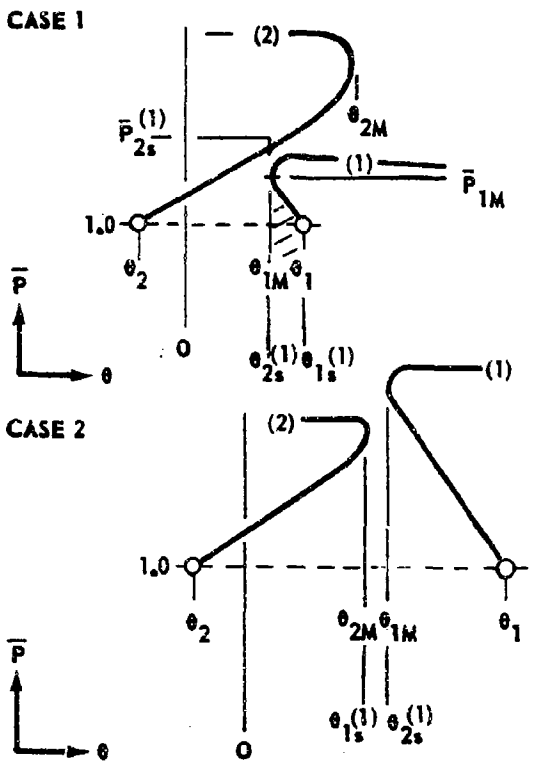

FIGURE A-7. NO-SOLUTION EXAMPLES

After the existence of a slip-line solution and the initial solution interval, $\left[\theta_{2s}^{(1)} - \theta_{1s}^{(1)}\right]$, have been established, convergence to the solution value of the slip-line angle θ_s can be rapidly achieved by a process of interval halving and successive reduction of the solution interval. The solution interval is reduced according to the sign of the normalized difference in the pressure ratio (Figure A-5),

$$d^{(n)} = \left[\bar{P}_1^{(n)} - \bar{P}_2^{(n)}\right] \Big/ \left[0.5\left(\bar{P}_1^{(n)} + \bar{P}_2^{(n)}\right)\right] . \qquad \text{(A-27)}$$

If $d^{(n)} < 0$, then $\theta_{1s}^{(n-1)}$ is replaced by $\theta_s^{(n)}$ and $\theta_{2s}^{(n)} = \theta_{2s}^{(n-1)}$. Or if $d^{(n)} > 0$, $\theta_{2s}^{(n-1)}$ is replaced by $\theta_s^{(n)}$ and $\theta_{1s}^{(n)} = \theta_{1s}^{(n-1)}$. This process is continued until

the solution criterion

$$\left| d^{(n)} \right| < \epsilon$$

is satisfied. Typically for $\epsilon = 10^{-5}$, convergence is achieved for $n < 10$.

Appendix B

METHOD OF CHARACTERISTICS

This appendix is based in part upon a previous report [6].

1. Basic Equations

For steady irrotational axisymmetric flow [3], the differential equation for the complete velocity potential in terms of the cylindrical coordinates (X, R) is

$$\left(1 - \frac{u^2}{C^2}\right)\frac{\partial^2\Phi}{\partial X^2} - 2\,\frac{uv}{C^2}\,\frac{\partial^2\Phi}{\partial X \partial R} + \left(1 - \frac{v^2}{C^2}\right)\frac{\partial^2\Phi}{\partial R^2} + \frac{\Phi}{R} = 0 \ , \qquad \text{(B-1)}$$

where

$$C^2 = C_0^2 - \frac{\gamma - 1}{2}\,(u^2 + v^2)\,; \quad V^2 = (u^2 + v^2) \qquad \text{(B-2)}$$

and

$$u = \frac{\partial\Phi}{\partial X}, \quad v = \frac{\partial\Phi}{\partial R} \ . \qquad \text{(B-3)}$$

The condition that the derivatives of:

$$\frac{\partial\Phi}{\partial X} \quad \text{and} \quad \frac{\partial\Phi}{\partial R}$$

may be discontinuous along curves on the solution surface to equation (B-1) $\left(\text{which implies that } \frac{\partial^2\Phi}{\partial X^2}\,,\ \frac{\partial^2\Phi}{\partial R^2}\,,\ \text{and } \frac{\partial^2\Phi}{\partial X \partial R} \text{ are indeterminate along such curves — the characteristic curves}\right)$ yields the following:

a) The physical characteristics:

$$\left(\frac{dR}{dX}\right)_{I,\,II} = \tan\,(\theta \mp \alpha) \qquad \text{(B-4)}$$

b) The hodograph characteristics:

$$(d\theta)_{I,II} \pm \frac{\cot \alpha}{V} (dV)_{I,II} \mp \frac{\sin \theta \sin \alpha}{\sin (\theta \mp \alpha)} \frac{(dR)_{I,II}}{R} = 0 \ . \qquad \text{(B-5)}$$

The Family I (right-running) and Family II (left-running) characteristics and the applicable notation are shown in Figure B-1.

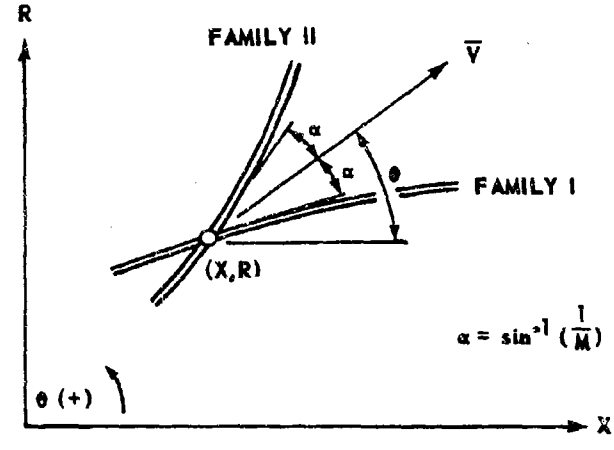

FIGURE B-1. PHYSICAL CHARACTERISTIC CURVES

Introduction of the velocity of sound at sonic conditions as a reference

$$C^* = \left[\frac{2\gamma \mathbb{R}}{\gamma + 1} \cdot T_o\right]^{1/2} \qquad \text{(B-6)}$$

and

$$M^* = V/C^* \qquad \text{(B-7)}$$

into equation (B-5), yields

$$(d\theta)_{I,II} \pm \frac{(dM^*)_{I,II}}{(M^* \tan \alpha)} \mp \frac{1}{R} \frac{\sin \theta \sin \alpha}{\sin (\theta \mp \alpha)} (dR)_{I,II} = 0 \ . \qquad \text{(B-8)}$$

The problem of solving equation (B-1) subject to the imposed boundary conditions then becomes equivalent to solving the set of simultaneous ordinary differential equations (B-4) and (B-8) under the same conditions. Various "unit processes" encountered in the numerical solution of equations (B-4) and (B-8) will now be discussed.

2. Field Points (FPS)

For two known points (1) and (2), Figure B-2, on the Family I and II characteristics, respectively, the location and flow variables at the unknown point (3) at the intersection of these characteristics can be determined by use of the characteristics relationships, equations (B-4) and (B-8).

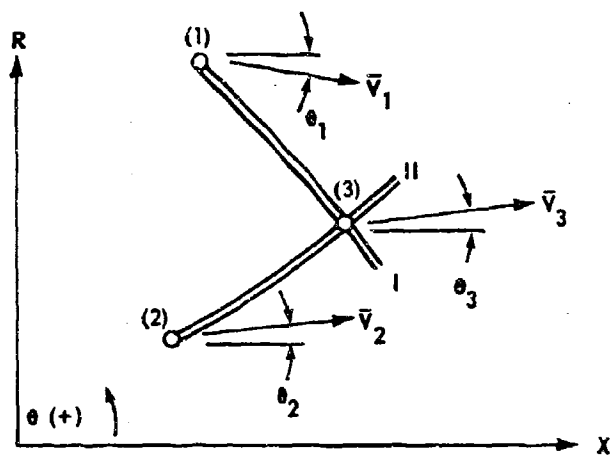

FIGURE B-2. GENERAL FIELD POINT

To a first approximation, the coordinates of point (3) are given in finite difference form as

$$X_3 = \frac{[(R_2 - R_1) + X_1 \tan(\theta - \alpha)_{13} - X_2 \tan(\theta + \alpha)_{23}]^{\dagger}}{[\tan(\theta - \alpha)_{13} - \tan(\theta + \alpha)_{23}]} \qquad \text{(B-9)}$$

---

†The notation $(\ )_{i3}$ indicates that average values between the points (i) and (3) are to be used.

and

$$R_3 = R_1 + (X_3 - X_1)\tan(\theta - \alpha)_{13} \tag{B-10}$$

where $[\theta + (-1)^i \alpha]_{i3}$ is defined as the average value of the quantity between the points (i = 1, 2) and (3). Correspondingly, the flow variables at (3) are given by:

$$\theta_3 = \frac{[P_{13}\theta_1 + P_{23}\theta_2 + (M_1^* - M_2^*) + Q_{13}(R_3 - R_1) - Q_{23}(R_3 - R_2)]}{[P_{13} + P_{23}]} \tag{B-11}$$

and

$$M_3^* = [M_1^* - P_{13}(\theta_3 - \theta_1) + Q_{13}(R_3 - R_1)] \quad , \tag{B-12}$$

where Q_{i3} and P_{i3} (i = 1 or 2) are coefficients based on the average values between the points (i) and (3).

These coefficients are defined as:

$$P_{i3} = (M^* \tan \alpha)_{i3} \tag{B-13}$$

and

$$Q_{i3} = P_{i3}\left[\frac{\sin\theta \sin\alpha}{R \sin[\theta + (-1)^i \alpha]}\right]_{i3} . \tag{B-14}$$

The values of $[X, R, M^*, \theta]_3$ are determined initially by assuming that the flow variables at point (3) are simply the average of those at points (1) and (2); hence,

$$\theta_3 = \frac{1}{2}(\theta_1 + \theta_2)$$

$$M_3^* = \frac{1}{2}(M_1^* + M_2^*) \quad .$$

Then by using equations (B-9) through (B-12) in sequential order, a first approximation to the values $[X, R, M^*, \theta]_3^{(1)}$ can be determined. These values are then used to determine the average quantities and subsequently the next approxi-

mation $[X, R, M^*, \theta]_3^{(2)}$. If this procedure of successive approximations is repeated, values for the variables at point (3) for two successive approximations (n - 1) and (n) will be obtained; i.e.,

$$[X, R, M^*, \theta]_3^{(n-1)} \quad \text{and} \quad [X, R, M^*, \theta]_3^{(n)} .$$

If the problem areas discussed below are not encountered, the values calculated by this procedure stabilize rapidly, and the iteration is terminated when

$$\left| \left[\theta_3^{(n)} - \theta_3^{(n-1)} \right] \Big/ \theta_3^{(n)} \right| \leq \epsilon_1 \tag{B-15}$$

or

$$\left| \left[M_3^{*(n)} - M_3^{*(n-1)} \right] \Big/ M_3^{*(n)} \right| \leq \epsilon_2 . \tag{B-16}$$

Typically for values of $\epsilon_1, \epsilon_2 = 10^{-4}$, the iteration stabilizes for $5 < n < 10$.

Difficulties encountered in the course of this iterative procedure have definite physical significance that can be traced to:

a) Either of the characteristics being oriented such that the quantity:

$$\left[\theta + (-1)^i \alpha \right]_{i3} \approx 0 \tag{B-17}$$

or, in other words, a characteristic is horizontal in the flow field for which

$$Q_{i3} \rightarrow \infty . \tag{B-18}$$

b) Compressions developed in the flow field due to wave coalescence such that

$$M_3^{*(n)} \leq 1 . \tag{B-19}$$

In the first case, the quantity

$$Q_{i3} \left(R_3 - R_i \right) \tag{B-20}$$

must be reconsidered when

$$\left[\theta + (-1)^i \alpha \right]_{i3} \rightarrow 0 . \tag{B-21}$$

The incremental length, $\Delta\ell$, along either characteristic is given by

$$\Delta\ell \approx \frac{\left(R_3 - R_i\right)}{\sin\left[\theta + (-1)^i \alpha\right]_{i3}} \qquad \text{(B-22)}$$

and as $\left[\theta + (-1)^i \alpha\right]_{i3} \to 0$, $\Delta\ell \to \left(X_3 - X_i\right)$. Hence, the quantity in the characteristics equations (B-11) and B-12) must then be replaced by the limiting value of equation (B-20), i.e.,

$$Q_{i3}\left(R_3 - R_i\right) \to P_{i3}\left[\frac{\sin\theta \sin\alpha}{R}\right]_{i3}\left(X_3 - X_i\right) \qquad \text{(B-23)}$$

when

$$\left[\theta + (-1)^i \alpha\right]_{i3} \to 0 \ . \qquad \text{(B-24)}$$

The second problem area usually results from "foldback" of the characteristics network as a result of the coalescence of the same family waves. To treat this problem, provisions must be made in the overall flow-field claculation sequence so that the shock formed in the flow field as a result of this coalescence can be treated and thus, "foldback" of the characteristics network avoided.

3. Axis Points (APS)

If any one of the points (1, 2, or 3) is located on the axis of symmetry, then,

$$R_j, \theta_j = 0 \qquad j = 1, 2, \text{ or } 3 \qquad \text{(B-25)}$$

and the calculation procedure of section 2 is modified accordingly for the axis point calculations. No particular problems are encountered when these conditions are imposed on the field-point calculation sequence since the term $[R^{-1}]$ only appears in the characteristic equations as an average value in the coefficients Q_{i3}.

The two axis point calculations encountered in the primary flow-field analysis are shown in Figure B-3.

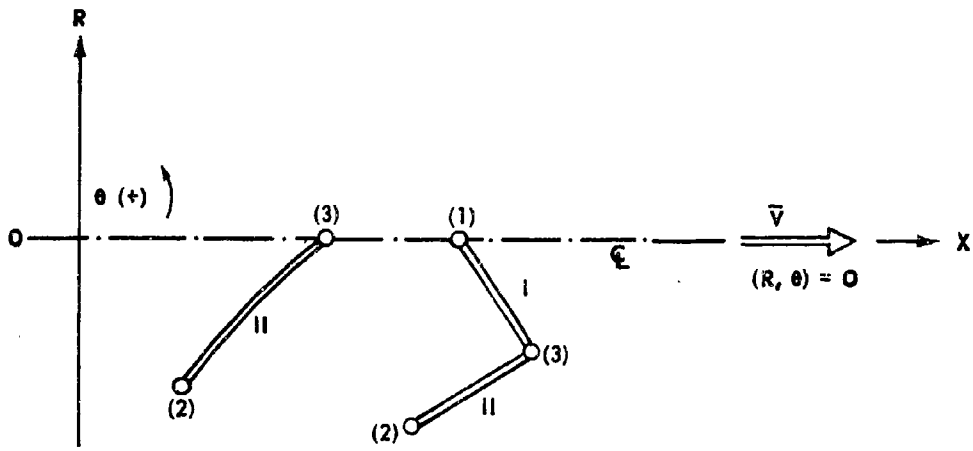

FIGURE B-3. AXIS POINTS

For the one case, the unknown point (3) is on the axis, and consequently,

$$R_3,\ \theta_3 = 0 \ . \tag{B-26}$$

Then the remaining values $[X, M^*]_3$ are found from:

$$X_3 = X_2 - \frac{R_2}{\tan\ (\theta + \alpha)_{23}} \tag{B-27}$$

$$M_3^* = M_2^* - P_{23}\theta_2 - Q_{23}P_2 \ . \tag{B-28}$$

To start the calculation sequence, it is assumed that

$$M_3^* = M_2^* \ .$$

Then a first approximation $[X, M^*]_3^{(1)}$ can be found from equations (B-27) and (B-28). Using the successive approximation technique, the calculations are continued until:

$$\left| \left[(M_3^*)^{(n)} - (M_3^*)^{(n-1)} \right] \Big/ M_3^{*(n)} \right| \leq \epsilon \ . \tag{B-29}$$

Thus the conditions at point (3) are determined as: $[X,\ 0,\ M^*, 0]_3^{(n)}$.

In the other case, the known point (2) is on the axis where:

$$R_2,\ \theta_2 = 0\ .$$

The calculation sequence for determining the values at point (3) are the same as outlined for the field-point analysis (section 2).

4. Boundary Points

For the base-flow analysis, only two types of boundary-point calculations occur, viz., the constant-pressure condition for the separated flow region and the solid boundary condition when an afterbody precedes the external stream's separation point.

a. Constant Pressure Boundary Points (CPBS)

Along the boundary (Figure B-4) the condition of constant pressure is expressed by:

$$M_3^* = M_2^* = M_B^* = \text{constant}, \tag{B-30}$$

where M_B^* is found from the isentropic flow function

$$\frac{P}{P_o}\left[\gamma, M_B^*\right] = \bar{P}_B = \text{constant}. \tag{B-31}$$

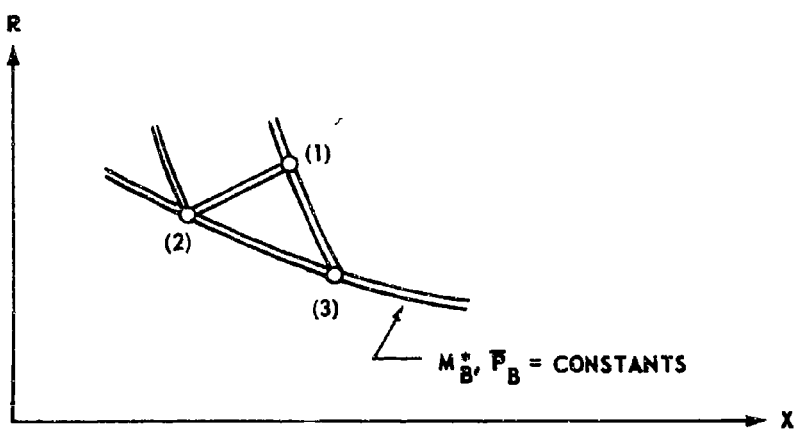

FIGURE B-4. CONSTANT-PRESSURE BOUNDARY POINT

A first approximation to the spatial location of the unknown point (3) is found from the streamline condition, between points (2) to (3), where

$$(R_3 - R_2) = (X_3 - X_2)\tan\theta_{23} \tag{B-32}$$

and along the I-characteristic, between points (1) to (3), where

$$(R_3 - R_1) = (X_3 - X_1)\tan(\theta - \alpha)_{13} \ . \tag{B-33}$$

Then X_3 is found from:

$$X_3 = \frac{[R_1 - R_2 + X_2 \tan\theta_{23} - X_1 \tan(\theta - \alpha)_{13}]}{[\tan\theta_{23} - \tan(\theta - \alpha)_{13}]} \ . \tag{B-34}$$

The local flow direction is then given by:

$$\theta_3 = \theta_1 - \frac{[(M_3^* - M_1^*) - Q_{13}^{\dagger}(R_3 - R_1)]}{P_{13}} \ . \tag{B-35}$$

The calculation sequence is initialized by assuming that

$$\theta_3 \approx \frac{1}{2}(\theta_1 + \theta_2) \ .$$

The corresponding values of $\left[X_3^{(1)}, R_3^{(1)}, \theta_3^{(1)}\right]$ are then found from equations (B-30), (B-34), (B-32), and (B-35). By use of these equations and the current approximations to the variables at point (3) to evaluate the average-value coefficients, the estimates for $[X, R, \theta]_3$ can be improved by successive approximations until

$$\left|\left[\theta_3^{(n)} - \theta_3^{(n-1)}\right] \Big/ \theta_3^{(n)}\right| < \epsilon \ .$$

Thus the variables at point (3) are determined as $[X, R, \theta]_3^{(n)}$ and $\left[M_3^* = M_B^*\right]$.

b. Solid-Boundary Points (BTBPS)

Along a solid boundary (Figure B-5) the flow must be tangent to the surface, and therefore at any point (3) on the surface, the local flow direction is given by:

$$\theta_3 = \tan^{-1}\left[\left(\frac{dR_s}{dX_s}\right)_3\right] \ . \tag{B-36}$$

$^{\dagger}Q_{13}$ is evaluated according to section 2, equations (B-14) or (B-23).

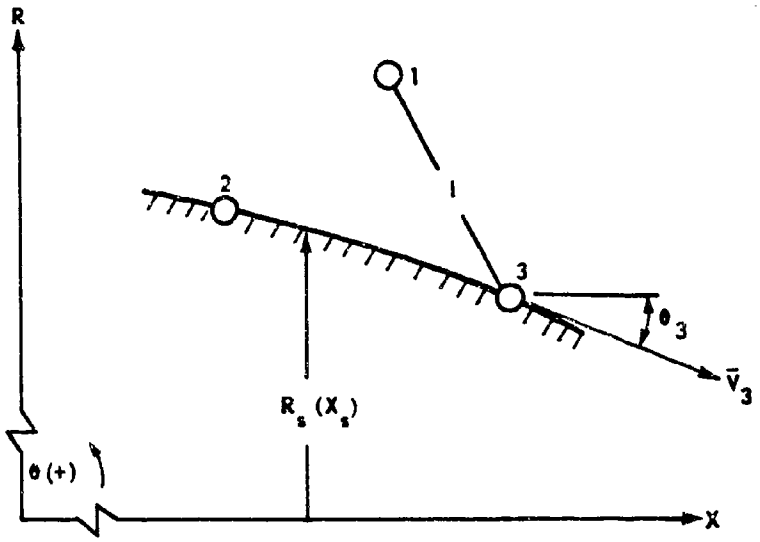

FIGURE B-5. SOLID-BOUNDARY POINT

The solid-boundary profile is assumed to be described in the meridional plane by a functional relationship of the form

$$R_s = R_s\left(X_s\right) \quad . \tag{B-37}$$

However, before the streamline condition specified by equation (B-36) can be applied, an initial estimate of the location of the unknown point (3) on the solid-boundary must be made. By assuming that the location and flow properties are known at a point (1) in the adjacent flow field and a point (2) on the solid-boundary, initial estimates of the flow properties at point (3) are

$$\theta_3 \approx \frac{1}{2}\left(\theta_1 + \theta_2\right) \tag{B-38}$$

$$M_3^* \approx \frac{1}{2}\left(M_1^* + M_2^*\right) \quad . \tag{B-39}$$

The approximate location of point (3) on the solid boundary is then found by solving simultaneously the physical I-characteristic relationship between points (1) and (3) and the equation specifying the boundary profile. The relationships to be solved are:

$$(R_3 - R_1) = (X_3 - X_1)\tan(\theta - \alpha)_{13} \qquad \text{(B-40)}$$

and

$$R_s = R_s(X_s) \qquad \text{(B-37)}$$

when $R_s = R_3$ and $X_s = X_3$. Carrying out this simultaneous solution and using equation (B-36) results in an approximate set of values for

$$[X, R, \theta]_3^{(1)} \quad .$$

By use of these data along with the hodograph I-characteristic relationship between points (1) and (3), the local value of M_3^* can be estimated from

$$M_3^* = M_1^* - P_{13}(\theta_3 - \theta_1) + PROD_{13} \qquad \text{(B-41)}$$

where for $|(\theta - \alpha)_{13}| > 0$ (cf. Field Point discussion),

$$PROD_{13} = Q_{13}(R_3 - R_1) \quad , \qquad \text{(B-42)}$$

or for $|(\theta - \alpha)_{13}| \approx 0$

$$PROD_{13} = P_{13}\left[\frac{\sin\theta \sin\alpha}{R}\right]_{13}(X_3 - X_1) \quad . \qquad \text{(B-43)}$$

Thus, the location and flow properties at point (3) for this first approximation are determined as:

$$[X, R, M^*, \theta]_3^{(1)} \quad .$$

For the next and all successive approximations, the $(n-1)^{th}$ estimates of $[M^*, \theta]_3^{(n-1)}$ are used with equations (B-40), (B-37), and (B-41) through (B-43) to determine the n^{th} estimates of $[X, R, M^*, \theta]_3^{(n)}$. This procedure is repeated until the normalized difference in M_3^* satisfies the convergence criterion:

$$\left|\left[M_3^{*(n)} - M_3^{*(n-1)}\right] \Big/ M_3^{*(n)}\right| < \epsilon^{\dagger} \qquad \text{(B-45)}$$

---

† For $\epsilon = 10^{-4}$, equation (B-45) is typically satisfied for $5 < n < 10$.

Thus when equation (B-45) is satisfied, the final values of

$$[X, R, M^*, \theta]_3^{(n)}$$

are determined.

5. Flow-Field Analysis (ACPBS)

The unit processes described above are organized into a sequential program which can be used to calculate the flow field subject to the imposed boundary conditions. This organization is principally one of "bookkeeping" and is normally not difficult. The basic sequence can take any of several different forms; the preference here has been to calculate along Family I characteristics toward the boundary.

a. Calculation Sequence

The boundary conditions imposed on the flow-field calculation (Figures B-6 through B-9) are:

1) The flow variables are specified along the initial internal (nozzle) flow or external (free stream) flow characteristic.

2) The conditions along the boundary are specified for the particular type of boundary condition that is being considered.

These data along with the surface geometry, if applicable, are sufficient to determine the flow field.

At the nozzle corner $\left(X_{1I}, R_{1I}\right)$ a centered expansion (or compression), can occur as a result of the need for the internal flow to expand (or compress) at the nozzle exit to satisfy the imposed constant-pressure boundary condition. A similar situation can also occur for the external (free stream) flow as a result of expansion (or compression) corners and a solid-boundary preceding the separation point of the external stream as well as the requirement that the external flow must adjust to the pressure level maintained downstream of the separation point. The general flow-field calculation sequence selected here for either the internal or external flow-field proceeds from the initial Family II characteristic (nozzle or afterbody) along I-characteristics to the boundary.

The calculation sequence for internal flow and external flow are illustrated in Figures B-6 and B-7, respectively.

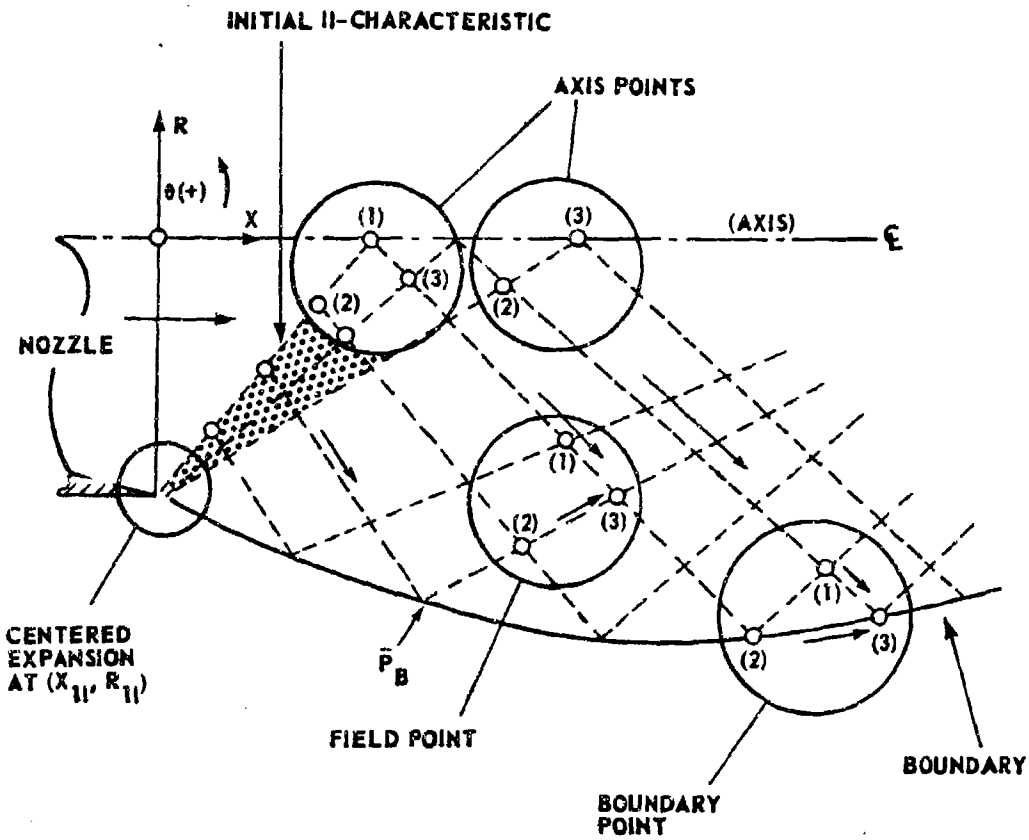

FIGURE B-6. FLOW-FIELD ANALYSIS

b. Wave Coalescence

The Family II characteristics from the internal constant-pressure boundary tend to steepen as the calculations proceed in the downstream direction. These characteristics eventually coalesce and form a shock wave within the flow field. This condition is detected by the crossing of waves of the same family thus giving rise to the "foldback" of the characteristics network. Although flow-field calculations where "foldback" occurs still yield results which are in reasonable agreement with experiment [7], the flow-field calculations must invariably be terminated as a result of errors directly attributable to the unrealistic characteristic network that develops.

An exact treatment of this problem has been given [8], as well as an approximate treatment [9]. However, since the calculated boundary is

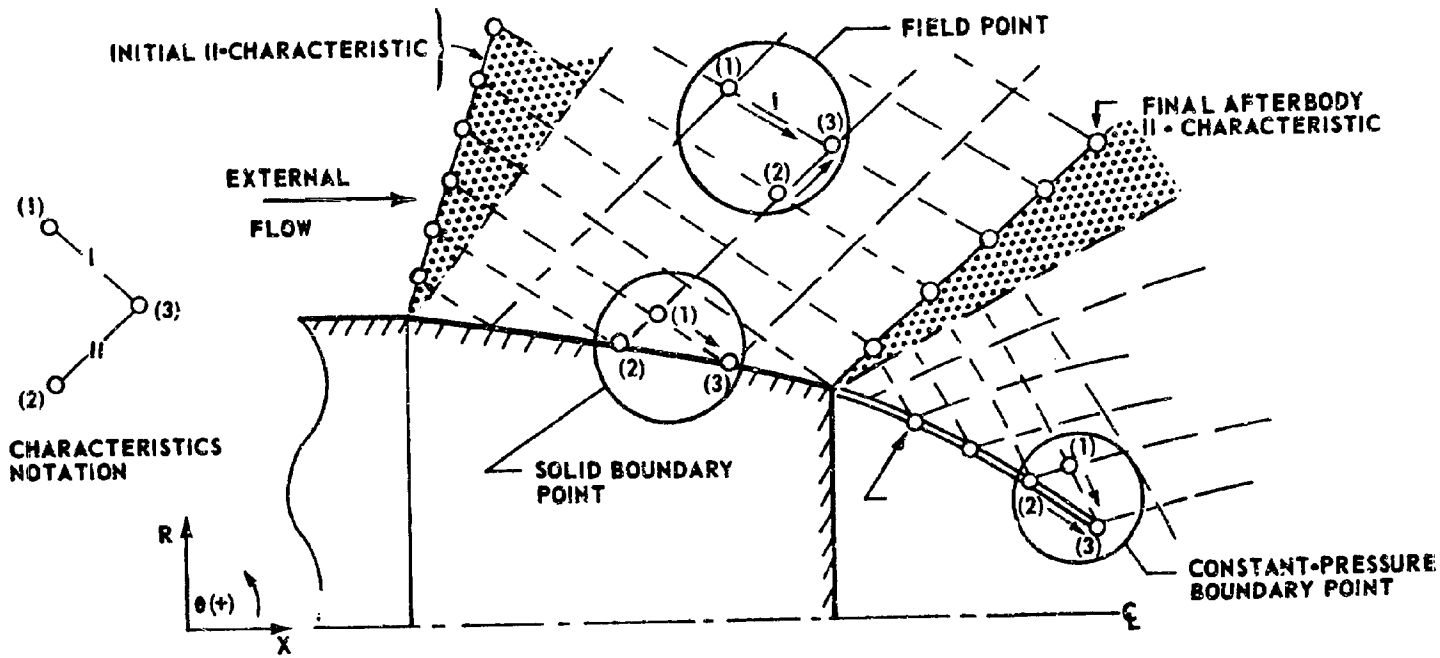

FIGURE B-7. EXTERNAL FLOW-FIELD ANALYSIS

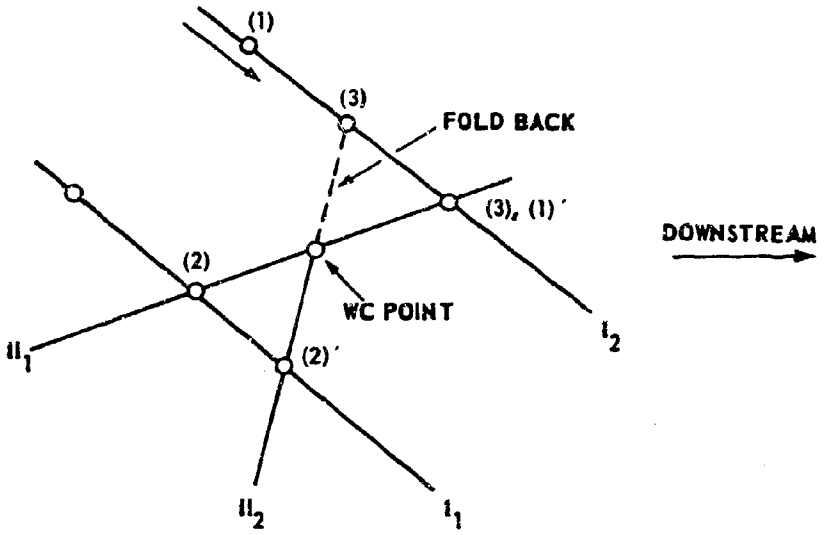

FIGURE B-8. SAME-FAMILY WAVE COALESCENCE

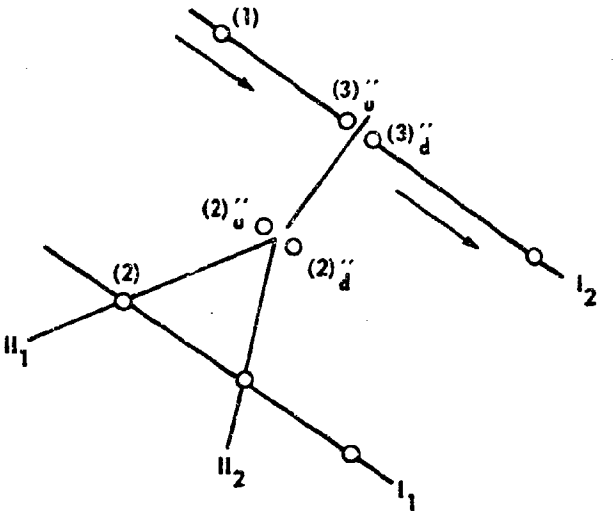

FIGURE B-9. MODIFICATION OF THE CALCULATION SEQUENCE FOR TREATING WAVE COALESCENCE

relatively insensitive to the method used to treat the coalescence problem, a simplified approach will be described here which is in excellent agreement with previous reports [8, 9].

In reference to Figure B-8, wave coalescence has occurred within the flow field. Allowing a single "foldback" at this point, the conditions on the "upstream" and "downstream" sides of the coalescence point are determined by linear interpolation between the points (2) and (3) and the points (2)' and (3)', respectively. The "foldback" points (3) and (3)' are then dropped and the flow-field calculations are continued by using the flow variables determined at the wave-coalescent point, Figure B-9.

In actuality, the oblique shock wave formed in the flow field due to the wave coalescence propagates downstream where it becomes curved as a result of the continuous interaction between the shock and the waves in the flow field. As a consequence, the flow is rotational downstream of the internal shock wave. In the approximation described above, the flow is assumed to remain irrotational. This assumption yields, in most cases, results which are acceptable and consistent with the overall analysis.

6. Initial Nozzle Characteristic

The nozzle geometries are restricted to those configurations which produce sonic, uniform, or conical supersonic flow. The objective is to determine the flow variables along the initial nozzle characteristic for each configuration.

a. Sonic Nozzle

The sonic nozzle can be treated approximately as a nozzle which produces uniform flow at the nozzle exit that is slightly supersonic, e.g., $M^*_{11} = 1.01$.

b. Uniform Supersonic Nozzle (UFLOC)

For uniform supersonic flow at the nozzle exit (Figure B-10) the initial I-characteristic is straight and the flow variables are known as $\left[M^*_{11}, \theta_{11} = 0\right]$ along this characteristic.

The case where an initial compression must exist at the nozzle exit to satisfy the imposed boundary condition will be considered, in an approximate way, in the subsection to follow, "A Compression at the Nozzle Exit."

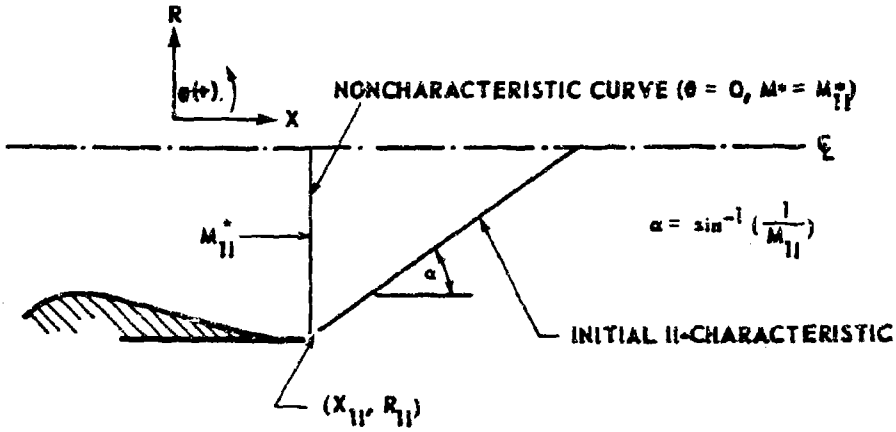

FIGURE B-10. UNIFORM SUPERSONIC FLOW NOZZLE

c. Conical Supersonic Nozzle (CNFLOC)

The flow in an ideal conical nozzle (Figure B-11) can be specified as being at a uniform Mach number $\left(\text{or } M^*_{II}\right)$ along the zone of the spherical sector that coincides with the nozzle. The initial I-characteristic can be determined exactly [10], or numerically from the flow conditions specified on the non-characteristic spherical surface.

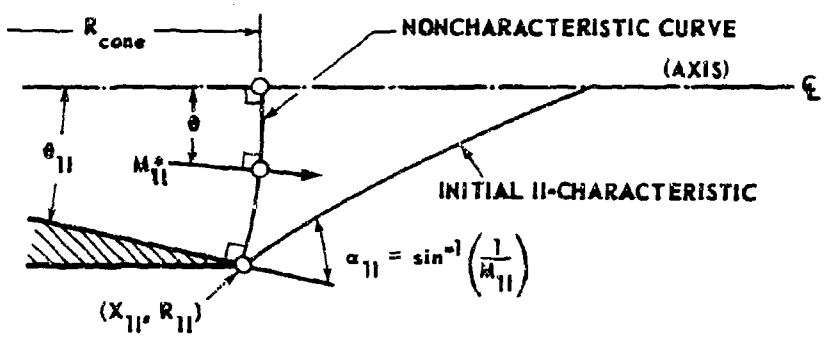

FIGURE B-11. CONICAL SUPERSONIC FLOW NOZZLE

The numerical approach while yielding values for the initial I-characteristic that are in excellent agreement with previous exact theoretical

results [10] has the advantage of being easily extended to treat approximately the problem of an initial compression at the nozzle exit (for both the uniform and conical nozzles).

The flow conditions are specified along the non-characteristic curve (Figure B-12) as being at a uniform value of M^*_{11} and that the velocity vector is always perpendicular to this curve. Any point on this curve is defined by $\left[X, R, M^*_{11}, \theta\right]_{NC}$ where $0 \geq \theta \geq \theta_{11}$ and

$$X = X_{11} + R_{cone}\left[\cos\theta - \cos\theta_{11}\right] \qquad \text{(B-46)}$$

$$R = R_{cone} \sin\theta \ , \qquad \text{(B-47)}$$

where

$$R_{cone} = R_{11}/\sin\theta_{11} \ . \qquad \text{(B-48)}$$

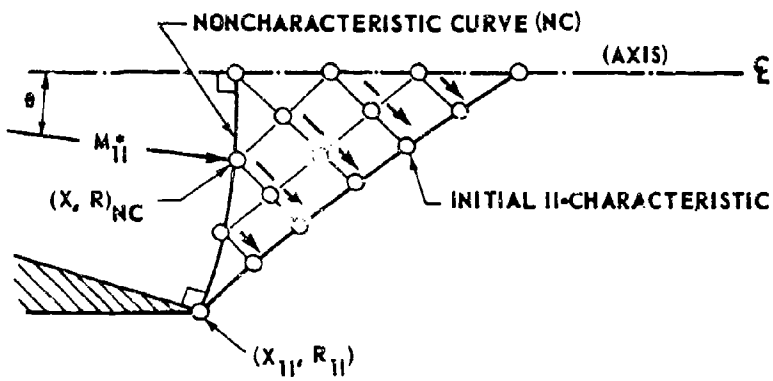

FIGURE B-12. CHARACTERISTICS NETWORK FOR NUMERICAL CALCULATION OF THE INITIAL II-CHARACTERISTICS FOR A CONICAL NOZZLE

The non-characteristic curve is then subdivided and a characteristics network (Figure B-12) can be used to determine numerically the flow variables and corresponding locations on the initial conical nozzle characteristic.

This general calculation sequence is useful since the calculations are made from a non-characteristic curve to the corresponding characteristic curve.

d. A Compression at the Nozzle Exit

If the boundary conditions are such that the nozzle discharges into a region at a pressure greater than the supersonic design pressure, an oblique shock wave is generated in the primary flow field. If this compression is assumed to be relatively weak, the oblique shock can be treated approximately as a reversible compression. For either the uniform or conical nozzle, the flow variables on the noncharacteristic curve and the imposed boundary conditions are used to establish a single reversible compression wave at the nozzle exit location (X_{II}, R_{II}) which satisfies the boundary conditions. With these data, the remainder of the initial I-characteristic can be established using the calculation sequence from the non-characteristic curve to the corresponding characteristic curve (Figure B-13).

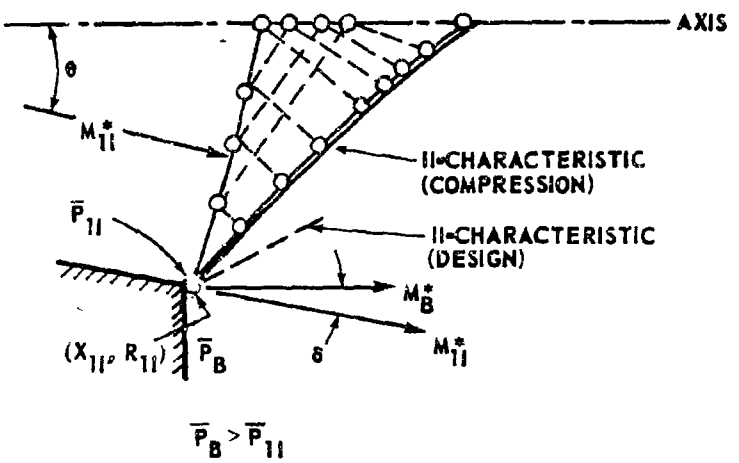

FIGURE B-13. APPROXIMATE ANALYSIS OF A COMPRESSION AT THE NOZZLE EXIT

7. Afterbody Analysis (ABTS)

The afterbody analysis utilizes the unit processes described in section 4; this analysis must, however, be consistent with the flow-field analysis of section 5a (Figure B-7). In addition to determining the detailed flow conditions over the afterbody, the final Family II-characteristic originating at the terminus of the afterbody must be determined so that the same flow-field calculation algorithm can be used for calculating both the external and internal flow fields and constant-pressure boundaries.

a. Initial and Final Family II Characteristics

The approach flow to the afterbody is currently restricted to uniform supersonic flow. For this case, the initial II-characteristic is a straight line along which the flow properties are constant and known at each arbitrarily selected subdivision point; this situation is shown in Figure B-14.

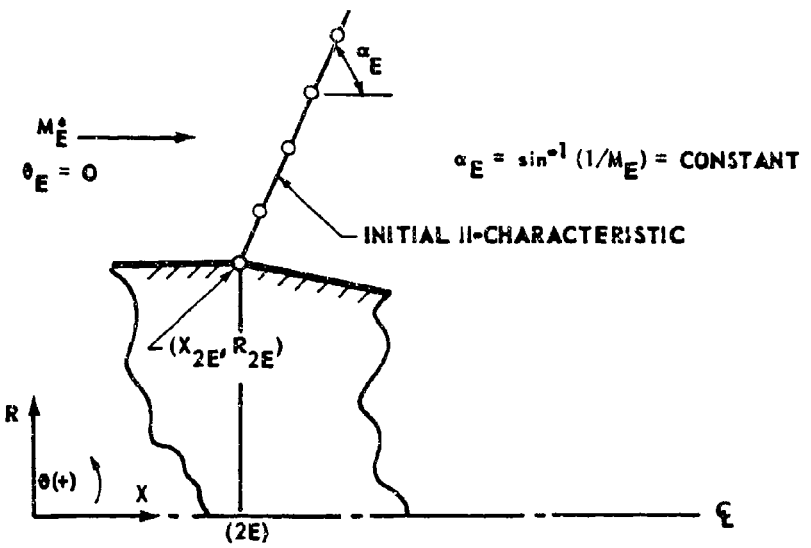

FIGURE B-14. INITIAL II-CHARACTERISTICS FOR UNIFORM EXTERNAL SUPERSONIC FLOW

When an afterbody is present, the points along the final II-characteristic originating at the afterbody terminus are determined as input data for the subsequent constant-pressure boundary calculations. After the I-characteristic originating at the initial II-characteristic and passing through the terminus of the body is found by iteration, the remainder of the points along the final II-characteristic are found by continuing to subdivide the initial II-characteristic and continuing the method of characteristics calculations to the final II-characteristic (Figure B-15).

b. Specific Afterbody Profiles (BTCNST)

As discussed in section 4b ("Solid-Boundary Points"), a simultaneous solution must be made between the equations describing the

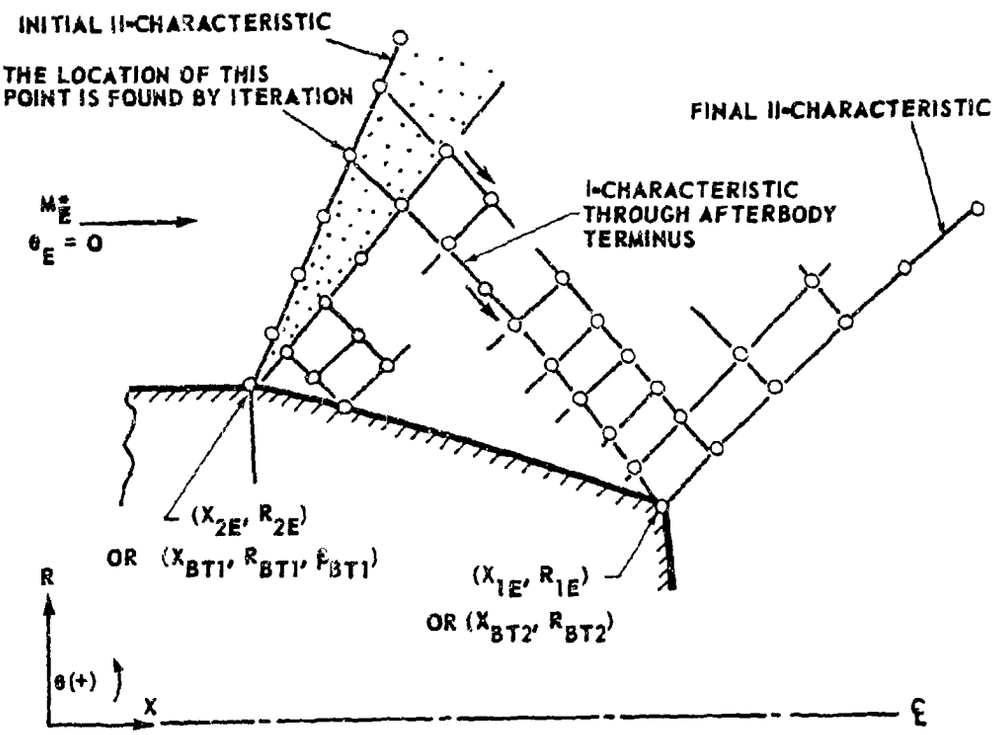

FIGURE B-15. DETERMINATION OF THE FINAL II-CHARACTERISTIC THROUGH THE AFTERBODY TERMINUS

afterbody profile and the physical I-characteristic; this solution determines points in the characteristic network which are located on the afterbody surface.

The purpose of this section is to summarize the resulting expressions for three afterbody shapes — the ogive (circular segment), the parabola, and the cone. A typical afterbody configuration and the associated notation are given in Figure B-16; for each shape, the afterbody is assumed to be completely specified by the values of

$$\left[X_{BT1},\ R_{BT1},\ \beta_{BT1}\right] \text{ and } \left[X_{BT2},\ R_{BT2}\right] .$$

The equations specifying the afterbody's meridional profile are summarized in Table B-I. The constants $[C_1, C_2, C_3]$ in the profile equations are determined for each afterbody based on the values specified at points (BT1) and (BT2). The resulting expressions for these constants are summarized in Table B-II.

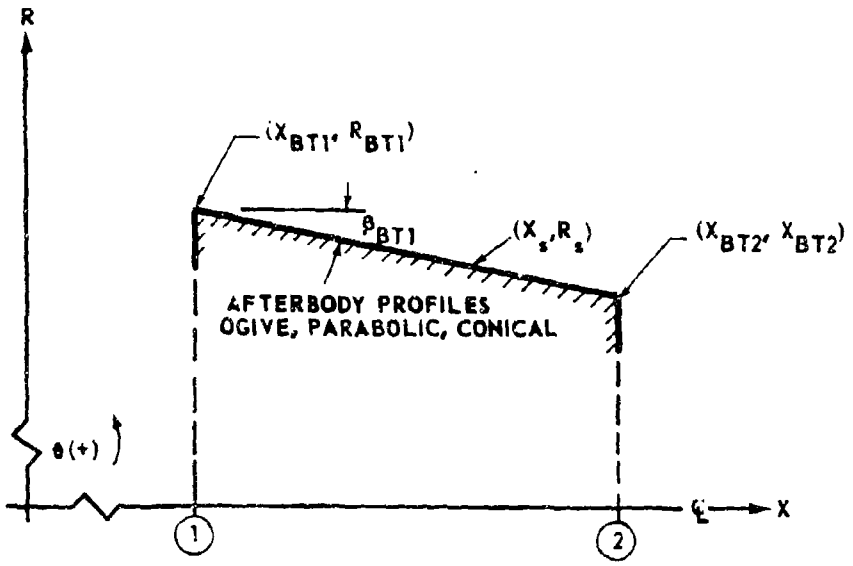

FIGURE B-16. GENERAL AFTERBODY NOTATION

TABLE B-I. EQUATIONS OF AFTERBODY MERIDIONAL-PLANE PROFILES

Shape	$R_s = R_s(X_s)$
Ogive	$R_s = C_1 + \left[C_3 - (X_s - C_2)^2\right]^{1/2}$
Parabolic	$R_s = C_3 + C_2 X_s + C_1 X_s^2$
Conical	$R_s = C_1 + C_2(X_s - C_3)$

The simultaneous solution of equations (B-37) and (B-40) has been carried out for the profiles specified in Table B-I; the results of these solutions are summarized in Table B-III.

TABLE B-II. CONSTANTS IN AFTERBODY PROFILE EQUATIONS

Shape	Constants $[C_1, C_2, C_3]$
Ogive	$C_1 = \frac{1}{2}\left\{\frac{\left[\left(X_{BT2} - X_{BT1}\right)^2 - 2\tan\beta_{BT1} R_{BT1}\left(X_{BT2} - X_{BT1}\right) + R_{BT2}^2 - R_{BT1}^2\right]}{\left[R_{BT2} - R_{BT1} - \tan\beta_{BT1}\left(X_{BT2} - X_{BT1}\right)\right]}\right\}$ $C_2 = X_{BT1} + \tan\beta_{BT1}\left(R_{BT1} - C_1\right)$ $C_3 = \left(X_{BT1} - C_2\right)^2 + \left(R_{BT1} - C_1\right)^2$
Parabolic	$C_1 = \left\{\frac{\left[R_{BT2} - R_{BT1} - \tan\beta_{BT1}\left(X_{BT2} - X_{BT1}\right)\right]}{\left(X_{BT2} - X_{BT1}\right)^2}\right\}$ $C_2 = \tan\beta_{BT1} - 2C_1 X_{BT1}$ $C_3 = R_{BT1} - \left(C_2 + C_1 X_{BT1}\right) X_{BT1}$
Conical	$C_1 = R_{BT1}$ $C_2 = \tan\beta_{BT1}$ $C_3 = X_{BT1}$

TABLE B-III. EXPRESSIONS FOR $[X_3, R_3, \theta_3]$ FROM THE SIMULTANEOUS SOLUTION OF EQUATIONS (B-37) AND (B-40) FOR VARIOUS AFTERBODY SHAPES

Shape	Simultaneous Solution Values for $[X_3, R_3, \theta_3]$
Ogive	$X_3 = \dfrac{\left\{- B - [B^2 - 4AC]^{1/2}\right\}}{2A}$ $A = 1 + \tan^2 (\theta - \alpha)_{13}$ $B = 2(R_1 - C_1)\tan (\theta - \alpha)_{13} - 2C_2 - 2X_1 \tan^2 (\theta - \alpha)_{13}$ $C = C_2^2 - C_3 + [(R_1 - C_1) - X_1 \tan (\theta - \alpha)_{13}]^2$ $R_3 = R_1 + (X_3 - X_1)\tan (\theta - \alpha)_{13}$ $\theta_3 = \tan^{-1}\left[\dfrac{(C_2 - X_3)}{(R_3 - C_1)}\right]$
Parabolic	$X_3 = \dfrac{\left\{- B - [B^2 - 4AC]^{1/2}\right\}}{2A}$ $A = C_1$ $B = C_2 - \tan (\theta - \alpha)_{13}$ $C = C_3 - R_1 + X_1 \tan (\theta - \alpha)_{13}$ $R_3 = R_1 + (X_3 - X_1)\tan (\theta - \alpha)_{13}$ $\theta_3 = \tan^{-1} [C_2 + 2C_1X_3]$
Conical	$X_3 = \dfrac{[C_1 - R_1 - C_2C_3 + X_1 \tan (\theta - \alpha)_{13}]}{[\tan (\theta - \alpha)_{13} - C_2]}$ $R_3 = R_1 + (X_3 - X_1)\tan (\theta - \alpha)_{13}$ $\theta_3 = \tan^{-1} (C_2) = \text{constant}$

Appendix C

MIXING ANALYSIS: TWO-DIMENSIONAL CONSTANT-PRESSURE TURBULENT MIXING

The general references for Appendixes C and D, although not cited, are several by Korst et al. [11-16].

1. Two-Dimensional Constant-Pressure Mixing Region

The two-dimensional mixing region control volume is shown in Figure C-1.

For constant-pressure mixing with:

a) uniform flow at x = 0

b) fully developed flow at x, the velocity profile within the mixing zone is given by

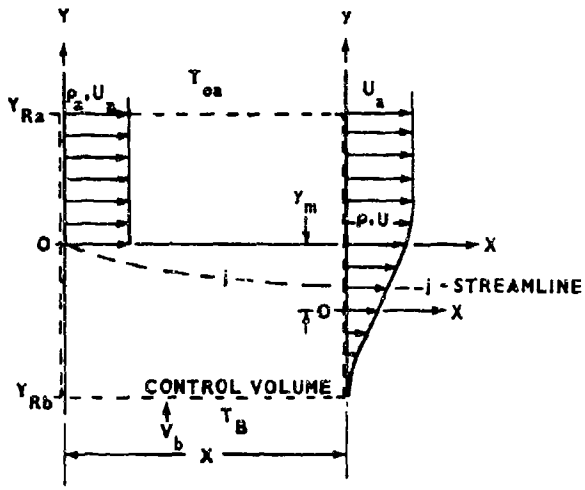

$$\phi = \frac{u}{U_a} = \frac{1}{2}\left[1 + \text{erf}\ \eta\right] ,$$

where

$$\eta = \frac{\sigma y}{x}$$

in which

(x,y) refer to the intrinsic coordinate system

σ = similarity parameter

$\sigma = 12 + 2.76\ M_a$.

FIGURE C-1. TWO-DIMENSIONAL MIXING REGION CONTROL VOLUME

2. Determination of y_m

The intrinsic coordinate system is located relative to the reference coordinates by applying the momentum equation in the x-direction (per unit width) to the control volume of Figure C-1. The result is:

$$-\rho_a U_a{}^2 Y_{RA} + \int_{Y_{Rb}}^{Y_{RA}} \rho u^2 dY = 0 \ , \qquad \text{(C-1)}$$

but

$$y = y_m(x) + Y$$

$$x \simeq X \ .$$

NOTES:

(a) $\int_0^x \rho V_b U_b dx = 0$,

since $U_b = 0$ at Y_{Rb}.

(b) At Y_{Ra}, the flow is undisturbed, and

(c) continuity equation applied to the control volume adds nothing.

Then

$$-\rho_a U_a{}^2 Y_{Ra} + \int_{\left(y_m+Y_{Rb}\right)}^{\left(y_m+Y_{Ra}\right)} \rho u^2 dy = 0 \ . \qquad \text{(C-2)}$$

Non-dimensionalizing with $\left(\rho_a, U_a\right)$,

$$-\eta_{Ra} + \int_{\eta_m+\eta_{Rb}}^{\eta_m+\eta_{Ra}} \frac{\rho}{\rho_a} \phi^2 d\eta = 0 \ , \qquad \text{(C-3)}$$

where

$$\eta = \sigma \frac{y}{x}$$

$$\phi = \frac{u}{U_a} \ .$$

Now at η_{Ra} and η_{Rb},

$$\left.\begin{aligned} &|1 - \phi| < \epsilon_a' \\ &|T_{ca} - T_o| < \epsilon_a'' \end{aligned}\right\} \text{ for } \eta \geq \eta_{ra} \qquad \text{(C-4)}$$

$$\left.\begin{aligned} &|\phi| < \epsilon_b' \\ &|T_B - T_o| < \epsilon_b'' \end{aligned}\right\} \text{ for } \eta \leq \eta_{Rb} \ . \qquad \text{(C-5)}$$

Therefore, equation (C-3) can be rearranged as

$$-\eta_{Ra} + \int_{\left(\eta_m+\eta_{Rb}\right)}^{\eta_{Rb}} \frac{\rho}{\rho_a}\,\phi^2 d\eta + \int_{\eta_{Rb}}^{\eta_{Ra}} \frac{\rho}{\rho_a}\,\phi^2 d\eta + \int_{\eta_{Ra}}^{\left(\eta_m+\eta_{Ra}\right)} \frac{\rho}{\rho_a}\,\phi^2 d\eta = 0 \qquad \text{(C-6)}$$

Thus

$$-\eta_{Ra} + \int_{\eta_{Rb}}^{\eta_{Ra}} \frac{\rho}{\rho_a}\,\phi^2 d\eta + \eta_m = 0 \qquad \text{(C-7)}$$

and consequently,

$$\eta_m = \eta_{Ra} - \int_{\eta_{Rb}}^{\eta_{Ra}} \frac{\rho}{\rho_a}\,\phi^2 d\eta \ . \qquad \text{(C-8)}$$

3. Identification of j-streamline

Application of the continuity equation to the jet flow yields

$$-\rho_a U_a Y_{RA} + \int_{Y_j}^{Y_{Ra}} \rho u\, dY = 0 \ . \qquad \text{(C-9)}$$

In non-dimensional form, equation (C-9) becomes:

$$-\eta_{Ra} + \int_{\eta_j}^{\eta_{Ra}+\eta_m} \frac{\rho}{\rho_a}\frac{u}{U_a}\, d\eta \qquad \text{(C-10)}$$

$$-\eta_{Ra} + \int_{\eta_j}^{\eta_{Ra}} \frac{\rho}{\rho_a}\,\phi d\eta + \int_{\eta_{Ra}}^{\eta_{Ra}+\eta_m} \frac{\rho}{\rho_a}\,\phi d\eta = 0 \ , \qquad \text{(C-11)}$$

or

$$\int_{\eta_j}^{\eta_{Ra}} \frac{\rho}{\rho_a}\,\phi d\eta = \left(\eta_{Ra} - \eta_m\right) \ , \qquad \text{(C-12)}$$

and combining equations (C-8) and (C-12), the integral equation to be solved for η_j is

$$\int_{\eta_j}^{\eta_{Ra}} \frac{\rho}{\rho_a}\,\phi d\eta = \int_{\eta_{Rb}}^{\eta_{Ra}} \frac{\rho}{\rho_a}\,\phi^2 d\eta \ . \qquad \text{(C-13)}$$

4. Energy Considerations

By use of Crocco's Integral Solution for an apparent unity turbulent Prandtl number, the stagnation temperature distribution in the mixing region is given by

$$\frac{T_o}{T_{oa}} = A + B\phi \qquad \text{(C-14)}$$

$$\left.\begin{aligned} \phi \to 0 \ , \ \frac{T_o}{T_{oa}} \to \frac{T_B}{T_{oa}} \ , \ \eta \to -\infty \\ \phi \to 1 \ , \ \frac{T_o}{T_{oa}} \to 1 \ , \ \eta \to \infty \end{aligned}\right\} \qquad \text{(C-15)}$$

$$A = \frac{T_B}{T_{oa}}$$

$$B = 1 - \frac{T_B}{T_{oa}}$$

$$\Lambda \equiv \frac{T_o}{T_{oa}} = \frac{T_B}{T_{oa}} + \left(1 - \frac{T_B}{T_{oa}}\right)\phi \qquad \text{(C-16)}$$

or

$$\Lambda = \Lambda_B + \left(1 - \Lambda_B\right)\phi \ , \qquad \text{(C-17)}$$

where

$$\Lambda_B \equiv \frac{T_B}{T_{oa}} \ . \qquad \text{(C-18)}$$

a. Energy Transferred Across j-Streamline

Shear work and conduction per unit width is

$$\int_{y_j}^{\left(Y_{Ra}+y_m\right)} \rho C_p \left(T_{oa} - T_o\right) u \, dy = e_j \ . \qquad \text{(C-19)}$$

In dimensionless form,

$$\frac{\sigma}{x} \frac{e_j}{\rho_a U_a C_p T_{oa}} = \int_{\eta_j}^{\left(\eta_{Ra}+\eta_m\right)} (1 - \Lambda) \frac{\rho}{\rho_a} \phi \, d\eta \ , \qquad \text{(C-20)}$$

since

$$(1 - \Lambda) \simeq 0 \quad \text{for} \quad \eta_{Ra} < \eta < \left(\eta_{Ra} + \eta_m\right)$$

equation (C-20) can be simplified as:

$$\frac{\sigma}{x}\frac{e_j}{\rho_a U_a C_p T_{oa}} = \int_{\eta_j}^{\eta_{Ra}} (1 - \Lambda)\frac{\rho}{\rho_a}\phi d\eta$$

$$= \int_{\eta_j}^{\eta_{Ra}} \frac{\rho}{\rho_a}\phi d\eta - \int_{\eta_j}^{\eta_{Ra}} \Lambda\frac{\rho}{\rho_a}\phi d\eta .$$

By use of equation (C-13),

$$\frac{\sigma}{x}\frac{e_j}{\rho_a U_a C_p T_{oa}} = \int_{\eta_{Rb}}^{\eta_{Ra}} \frac{\rho}{\rho_a}\phi^2 d\eta - \int_{\eta_j}^{\eta_{Ra}} \Lambda\frac{\rho}{\rho_a}\phi d\eta$$

$$= \int_{\eta_{Rb}}^{\eta_j} \frac{\rho}{\rho_a}\phi^2 d\eta + \int_{\eta_j}^{\eta_{Ra}} \frac{\rho}{\rho_a}\phi^2 d\eta - \int_{\eta_j}^{\eta_{Ra}} \Lambda\frac{\rho}{\rho_a}\phi\, d\eta$$

$$= \int_{\eta_{Rb}}^{\eta_j} \frac{\rho}{\rho_a}\phi^2 d\eta + \int_{\eta_j}^{\eta_{Ra}} \frac{\rho}{\rho_a}[\phi^2 - \Lambda\phi]d\eta$$

$$\frac{\sigma}{x}\frac{e_j}{\rho_a U_a C_p T_{oa}} = \int_{\eta_{Rb}}^{\eta_j} \frac{\rho}{\rho_a}\phi^2 d\eta + \int_{\eta_j}^{\eta_{Ra}} \frac{\rho}{\rho_a}\left[\phi^2 - \Lambda_B\phi - \left(1 - \Lambda_B\right)\phi^2\right]d\eta$$

$$= \int_{\eta_{Rb}}^{\eta_j} \frac{\rho}{\rho_a}\phi^2 d\eta + \int_{\eta_j}^{\eta_{Ra}} \frac{\rho}{\rho_a}\left[-\Lambda_B\phi + \Lambda_B\phi^2\right]d\eta$$

$$= \int_{\eta_{Rb}}^{\eta_j} \frac{\rho}{\rho_a}\phi^2 d\eta + \int_{\eta_j}^{\eta_{Ra}} \frac{\rho}{\rho_a}[\phi^2 - \phi_1\Lambda_B d\eta .$$

Also from equation (C-13),

$$\int_{\eta_j}^{\eta_{Ra}} \frac{\rho}{\rho_a}\,\phi d\eta = \int_{\eta_{Rb}}^{\eta_{Ra}} \frac{\rho}{\rho_a}\,\phi^2 d\eta = \int_{\eta_{Rb}}^{\eta_j} \frac{\rho}{\rho_a}\,\phi^2 d\eta + \int_{\eta_j}^{\eta_{Ra}} \frac{\rho}{\rho_a}\,\phi^2 d\eta \ .$$

Therefore,

$$\int_{\eta_j}^{\eta_{Ra}} \frac{\rho}{\rho_a}\,[\phi^2 - \phi]d\eta = -\int_{\eta_{Rb}}^{\eta_j} \frac{\rho}{\rho_a}\,\phi^2 d\eta \ ,$$

and continuing the simplification, the dimensionless energy transfer rate becomes:

$$\frac{\sigma}{x}\frac{e_j}{\rho_a C_p \overline{U}_a T_{oa}} = \int_{\eta_{Rb}}^{\eta_j} \frac{\rho}{\rho_a}\,\phi^2 d\eta - \Lambda_B \int_{\eta_{Rb}}^{\eta_j} \frac{\rho}{\rho_a}\,\phi^2 d\eta$$

$$= \int_{\eta_{Rb}}^{\eta_j} \left[\left(1 - \Lambda_B\right)\phi\right]\frac{\rho}{\rho_a}\,\phi d\eta \ . \qquad \text{(C-21)}$$

From equation (C-17)

$$\Lambda = \Lambda_B + \left(1 - \Lambda_B\right)\phi \quad \text{or} \quad \left[\left(1 - \Lambda_B\right)\phi\right] = \left(\Lambda - \Lambda_B\right) \ ,$$

hence, equation (C-21) can be expressed as:

$$\frac{\sigma}{x}\frac{e_j}{\rho_a U_a C_p T_{oa}} = \int_{\eta_{Rb}}^{\eta_j} \left(\Lambda - \Lambda_B\right)\frac{\rho}{\rho_a}\,\phi d\eta \qquad \text{(C-22)}$$

b. Energy Convected with Mass Between (j) and (d) Streamlines (with Reference to Zero Temperature) per Unit Width

The energy convected is:

$$e_d = \int_{y_j}^{y_d} \rho C_p u T_o dy \qquad \text{(C-23)}$$

or in dimensionless form

$$\frac{\sigma}{x} \frac{e_d}{\rho_a C_p U_a T_{oa}} = \int_{\eta_j}^{\eta_d} \frac{\rho}{\rho_a} \Lambda \phi d\eta$$

and finally expanding the integral

$$\frac{\sigma}{x} \frac{e_d}{\rho_a C_p U_a T_{oa}} = \int_{\eta_{Rb}}^{\eta_d} \frac{\rho}{\rho_a} \Lambda \phi d\eta + \int_{\eta_j}^{\eta_{Rb}} \frac{\rho}{\rho_a} \Lambda \phi d\eta \ . \qquad \text{(C-24)}$$

If $\lambda = \eta_{Rb} - \eta + \eta_j$, then

$$d\lambda = -d\eta$$

and the last integral in equation (C-24) can be expressed as:

$$\int_{\eta_j}^{\eta_{Rb}} \frac{\rho}{\rho_a} \Lambda \phi d\eta = - \int_{\eta_{Rb}}^{\eta_j} \frac{\rho}{\rho_a} \Lambda \phi d\lambda$$

since

$$\phi(\eta) \rightarrow \phi \left[\left(\eta_{Rb} + \eta_j \right) - \lambda \right] > 0 \quad \text{for} \quad \eta_{Rb} < \lambda < \eta_j$$

and

$$\Lambda > 0 ,$$

$$\frac{\rho}{\rho_a} > 0 .$$

Therefore, the dimensionless convected energy transfer rate is given by:

$$\frac{\sigma}{x} \frac{e_d}{\rho_a C_p U_a T_{oa}} = \int_{\eta_{Rb}}^{\eta_d} \frac{\rho}{\rho_a} \Lambda \phi d\eta - \int_{\eta_{Rb}}^{\eta_j} \frac{\rho}{\rho_a} \Lambda \phi d\eta \quad . \tag{C-25}$$

The total rate of energy transfer per unit width to the wake is found by combining equations (C-21) and (C-25). The result in dimensionless form is

$$\frac{\sigma}{x} \frac{e}{\rho_a C_p U_a T_{oa}} = \frac{\sigma}{x \rho_a C_p U_a T_{oa}} \left(e_j + e_d \right) \tag{C-26}$$

$$\frac{\sigma}{x} \frac{e}{\rho_a C_p U_a T_{oa}} = - \Lambda_B \int_{\eta_{Rb}}^{\eta_j} \frac{\rho}{\rho_a} \phi d\eta + \int_{\eta_{Rb}}^{\eta_d} \frac{\rho}{\rho_a} \Lambda \phi d\eta \tag{C-27}$$

5. Mass Transfer

Mass rate convected between (j) and (d) streamlines per unit with width is

$$g_d = \int_{y_j}^{y_d} \rho u \, dy , \tag{C-28}$$

or in dimensionless form

$$\frac{\sigma g_d}{x\rho_a u_a} = \int_{\eta_{Rb}}^{\eta_d} \frac{\rho}{\rho_a}\,\phi\,d\eta - \int_{\eta_{Rb}}^{\eta_j} \frac{\rho}{\rho_a}\,\phi\,d\eta \quad . \tag{C-29}$$

Equations (C-13), (C-27), and (C-29) define results for mixing analysis after ϕ and $\frac{\rho}{\rho_a}$ are determined.

6. Constant-Pressure Mixing

For an ideal gas, the equation of state is

$$P = \rho \mathbb{R} T \quad ;$$

then for P = constant,

$$\rho_a T_a = \rho T \tag{C-30}$$

or

$$\frac{\rho}{\rho_a} = \frac{T_a}{T} = \frac{T_a}{T_{oa}}\left(\frac{T_{oa}}{T_o}\right)\frac{T_o}{T} = \frac{T_a}{T_{oa}}\,\frac{1}{\Lambda}\,\frac{T_o}{T} \quad . \tag{C-31}$$

From the energy equation

$$T + \frac{u^2}{2C_p} = T_o$$

or

$$T + \left(\frac{u}{U_a}\right)^2\left(\frac{U_a^{\,2}}{2C_p T_{oa}}\right)T_{oa} = T_o \quad . \tag{C-32}$$

Defining the free stream Crocco number squared as

$$C_a^2 \equiv \frac{U_a^2}{2C_p T_{oa}}$$

$$\frac{u}{U_a} = \phi$$

$$T + C_a^2 \phi^2 T_{oa} = T_o \ , \qquad \text{(C-33)}$$

at "a,"

$$T_a + C_a^2 \, T_{oa} = T_{oa} \ .$$

Therefore,

$$\frac{T_a}{T_{oa}} = \left(1 - C_a^2\right) \ ; \qquad \text{(C-34)}$$

at any ϕ,

$$\frac{T_o}{T} = 1 + C_a^2 \phi^2 \, \frac{T_{oa}}{T_o} \left(\frac{T_o}{T}\right)$$

$$\frac{T_o}{T}\left[1 - \frac{C_a^2 \phi^2}{\Lambda}\right] = 1$$

$$\frac{T_o}{T} = \frac{\Lambda}{\left(\Lambda - C_a^2 \phi^2\right)} \ . \qquad \text{(C-35)}$$

Therefore, from equations (C-31), (C-34), and (C-35),

$$\frac{\rho}{\rho_a} = \left(1 - C_a^2\right) \frac{1}{\Lambda} \, \frac{\Lambda}{\left(\Lambda - C_a^2 \phi^2\right)} \qquad \text{(C-36)}$$

$$\frac{\rho}{\rho_a} = \frac{\left(1 - C_a^2\right)}{\left(\Lambda - C_a^2 \phi^2\right)} \ . \qquad \text{(C-37)}$$

7. Defined Integral Notation

The integral notation is defined by the following equations:

$$I_1(\eta) \equiv \int_{\eta_{Rb}}^{\eta} \frac{\phi}{\left(\Lambda - C_a^2\phi^2\right)} d\eta = I_1\left(\eta, \Lambda_B, C_a^2\right) \qquad (C\text{-}38)$$

$$I_2(\eta) \equiv \int_{\eta_{Rb}}^{\eta} \frac{\phi^2}{\left(\Lambda - C_a^2\phi^2\right)} d\eta = I_2\left(\eta, \Lambda_B, C_a^2\right) \qquad (C\text{-}39)$$

$$I_3(\eta) \equiv \int_{\eta_{Rb}}^{\eta} \frac{\Lambda\phi}{\left(\Lambda - C_a^2\phi^2\right)} d\eta = I_3\left(\eta, \Lambda_B, C_a^2\right) \qquad (C\text{-}40)$$

where

$$\Lambda = \frac{T_o}{T_{oa}} = \Lambda_B + \left(1 - \Lambda_B\right)\phi \ .$$

8. Equation Summary

The equation to be solved for η_j is:

$$\int_{\eta_j}^{\eta_{Ra}} \frac{\rho}{\rho_a}\phi d\eta = -\int_{\eta_{Rb}}^{\eta_j} \frac{\rho}{\rho_a}\phi d\eta + \int_{\eta_{Rb}}^{\eta_{Ra}} \frac{\rho}{\rho_a}\phi d\eta = \int_{\eta_{Rb}}^{\eta_{Ra}} \frac{\rho}{\rho_a}\phi^2 d\eta \qquad (C\text{-}13)$$

or in terms of the defined integrals, equations (C-38) and (C-39)

$$I_1\left(\eta_j\right) = \left[I_1\left(\eta_{Ra}\right) - I_2\left(\eta_{Ra}\right)\right] \ . \qquad (C\text{-}41)$$

The relationship between I_3 and I_1, I_2 is

$$I_3 = \int_{\eta_{Rb}}^{\eta} \frac{\Lambda\phi}{\left(\Lambda - C_a^2\phi^2\right)} d\eta = \Lambda_B \int_{\eta_{Rb}}^{\eta} \frac{\phi}{\left(\Lambda - C_a^2\varphi^2\right)} d\eta + \left(1 - \Lambda_B\right)\int_{\eta_{Rb}}^{\eta} \frac{\phi^2}{\left(\Lambda - C_a^2\phi^2\right)} d\eta$$

or in terms of the defined integral notation,

$$I_3 = \Lambda_B I_1 + \left(1 - \Lambda_B\right) I_2 \ .$$

From equation (C-27), the energy transfer rate becomes

$$\frac{\sigma e}{\left(1 - C_a^2\right) x \rho_a C_p U_a T_{oa}} = \left[I_3\left(\eta_d\right) - \Lambda_B I_1\left(\eta_j\right) \right] . \qquad \text{(C-42)}$$

From equation (C-29), the entrained mass rate is

$$\frac{\sigma g_d}{\left(1 - C_a^2\right) x \rho_a U_a} = \left[I_1\left(\eta_d\right) - I_1\left(\eta_j\right) \right] . \qquad \text{(C-43)}$$

9. d-Streamline Velocity Ratio

For the d-streamline, the recompression criterion yields a value of the d-streamline Crocco number, C_d. The value of C_d, the adjacent free stream data, and the state of the quiescent fluid can then be used to determine the d-streamline velocity ratio ϕ_d. This is accomplished in the following way.

The definition of the velocity ratio is considered:

$$\phi_d \equiv u_d / U_a \qquad \text{(C-44)}$$

or rearranging in terms of the corresponding Crocco numbers,

$$\phi_d = \left[\frac{u_d / \sqrt{2 C_p T_{od}}}{U_a / \sqrt{2 C_p T_{oa}}} \right] \sqrt{\frac{T_{od}}{T_{oa}}} = \frac{C_d}{C_a} \sqrt{\frac{T_{od}}{T_{oa}}} \ . \qquad \text{(C-45)}$$

The stagnation temperature ratio can be expressed from equation (C-16) as

$$\frac{T_{od}}{T_{oa}} = \Lambda_d = \Lambda_B + \left(1 - \Lambda_B\right) \phi_d \ , \qquad \text{(C-46)}$$

where

$$\Lambda_B = T_B / T_{oa} \ .$$

Therefore by combining equations (C-45) and (C-46), the expression to be solved for ϕ_d is

$$\phi_d = \frac{C_d}{C_a}\left[\Lambda_B + \left(1 - \Lambda_B\right)\phi_d\right]^{1/2} . \qquad \text{(C-47)}$$

Solving for ϕ_d, the result is

$$\phi_d = \frac{C_{nr}}{2}\left\{C_{nr}\left(1 - \Lambda_B\right) + \sqrt{C_{nr}^2\left(1 - \Lambda_B\right)^2 + 4\Lambda_B}\right\} \qquad \text{(C-48)}$$

where the ratio of the Crocco numbers has been defined as

$$C_{nr} \equiv C_d/C_a . \qquad \text{(C-49)}$$

Appendix D

MIXING ANALYSIS: APPLICATION OF THE TWO-DIMENSIONAL MIXING ANALYSIS TO THE TWO-STREAM AXISYMMETRIC BASE-PRESSURE PROBLEM

The approximate two-stream flow model is shown in Figure D-1.

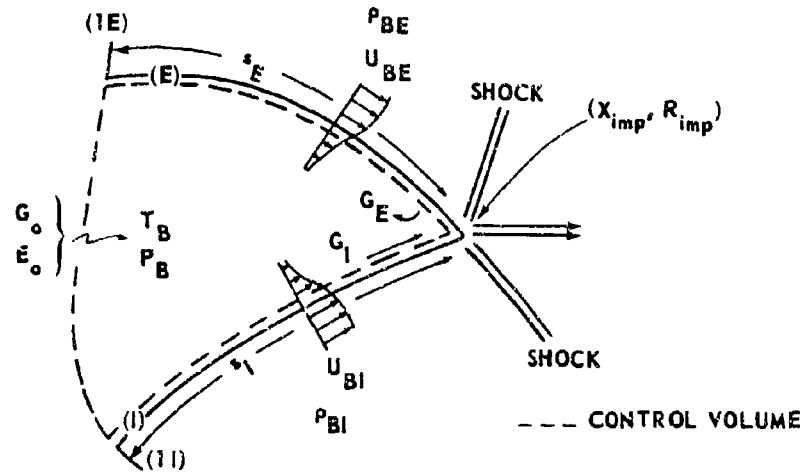

FIGURE D-1. APPROXIMATE TWO-STREAM FLOW MODEL

1. Two-Dimensional Approximation of the Mass and Energy Transfer Rates

Superposition of the two-dimensional mixing region on the "corresponding" inviscid flow field at the impingement point (Appendix C) of Figure D-1 is shown.

a. External Stream

The approximate entrained mass flow rate is determined from equation (C-43) as

$$G_E = 2\pi R_{imp}\left(1 - C_{BE}^2\right)\frac{s_E}{\sigma_E}\rho_{BE}U_{BE}\left[I_1\left(\eta_{dE}\right) - I_1\left(\eta_{jE}\right)\right] \quad . \quad (D\text{-}1)$$

The approximate energy transfer rate is determined from equation (C-42) as:

$$E_E = 2\pi R_{imp}\left(1 - C_{BI}^2\right)\frac{s_E}{\sigma_E}\rho_{BE}U_{BE}C_{pE}T_{oE}\left[I_3\left(\eta_{dE}\right) - A_{BE}I_1\left(\eta_{jE}\right)\right] , \tag{D-2}$$

where $A_{BE} = T_B / T_{oE}$.

b. Internal Stream

The entrained mass flow rate is (equation C-43)

$$G_I = 2\pi R_{imp}\left(1 - C_{BI}^2\right)\frac{s_I}{\sigma_I}\rho_{BI}U_{BI}\left[I_1\left(\eta_{dI}\right) - I_1\left(\eta_{jI}\right)\right] . \tag{D-3}$$

The energy transfer rate is (equation C-42)

$$E_I = 2\pi R_{imp}\left(1 - C_{BI}^2\right)\frac{s_I}{\sigma_I}\rho_{BI}U_{BI}C_{pI}T_{oI}\left[I_3\left(\eta_{dI}\right) - A_{BI}I_1\left(\eta_{jI}\right)\right] , \tag{D-4}$$

where $A_{BI} = T_B / T_{oI}$.

2. Conservation of Mass

For the base-region control volume, conservation of mass requires that

$$G_o + G_E + G_I = 0 . \tag{D-5}$$

The term G_o is a mass flow rate entering the base region at a negligible velocity, i.e., "mass bleed." By introduction, as a reference, of the internal stream's (nozzle flow) mass flow rate, G_{NI}, equation (D-5) can be written in dimensionless form as

$$\bar{B}_o + \bar{B} = 0 , \tag{D-6}$$

where the "bleed ratios" are defined by

$$\bar{B}_o \equiv G_o/G_{N1} \tag{D-7}$$

$$\bar{B} \equiv -\left(G_E + G_I\right)/G_{N1} \ . \tag{D-8}$$

3. Conservation of Energy

For the base region control volume, conservation of energy requires that

$$E_o + \left(E_E + E_I\right) = 0 \ . \tag{D-9}$$

By use of the total enthalpy of the internal stream (nozzle flow) as a reference, i.e.,

$$E_{N1} \equiv G_{N1} C_{pl} T_{ol} \ , \tag{C-10}$$

equation (D-8) can be written in dimensionless form as

$$\bar{E}_o - \bar{E} = 0 \ , \tag{D-11}$$

where

$$\bar{E}_o \equiv E_o/E_{N1} \tag{D-12}$$

$$\bar{E} \equiv -\left(E_E + E_I\right)/E_{N1} \ . \tag{D-13}$$

Thus for conservation of mass and energy in the base region, equations (D-6) and (D-11) must be simultaneously satisfied.

4. Nozzle Mass Flow Rate, G_{N1}

Figure D-2 presents the ideal nozzles and their notation.

For source flow through the conical nozzle (Figure D-2a) the flow Mach number is a constant over the nozzle's exit area and the velocity vector is always perpendicular to this area. The exit flow area is equal to the area of the zone of a sphere of radius R_N. The exit area is found as:

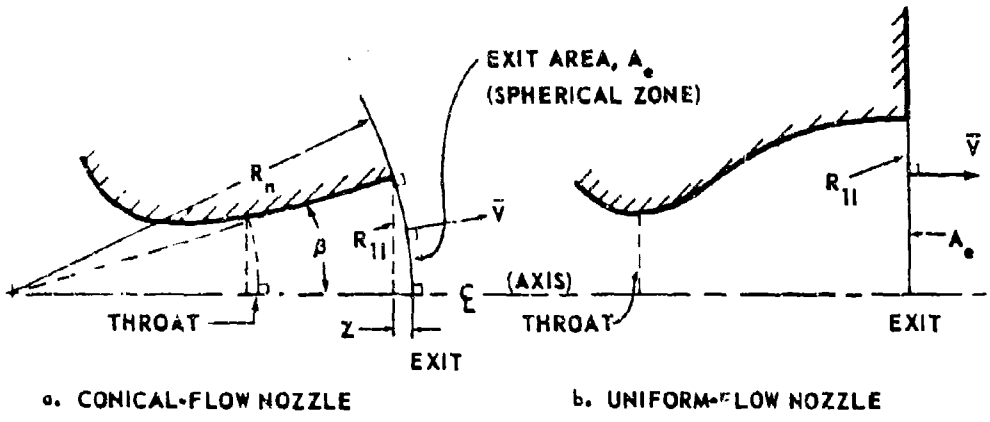

a. CONICAL-FLOW NOZZLE b. UNIFORM-FLOW NOZZLE

FIGURE D-2. IDEAL NOZZLES AND THEIR NOTATION

$$R_N = R_{II}/\sin\beta \tag{D-14}$$

$$Z = R_N(1 - \cos\beta) \tag{D-15}$$

$$A_e = 2\pi R_N Z = \frac{2\pi R_{II}^2}{(1 + \cos\beta)} \tag{D-16}$$

For the uniform flow nozzle (Figure D-2b) the exit flow area is given by

$$A_e = \pi R_{II}^2 \ . \tag{D-17}$$

Thus, for either conical ($\beta > 0$) or uniform ($\beta = 0$) flows, the nozzle exit flow area is given by

$$A_e = \frac{2\pi}{(1 + \cos\beta)} R_{II}^2 \ . \tag{D-18}$$

If the flow is uniform and one dimensional over the nozzle exit flow area, the ideal nozzle mass flow rate is given by

$$\frac{G_{NI}\sqrt{T_{oI}}}{P_{II}A_{II}} = \sqrt{\frac{\gamma_I g_c}{\mathbb{R}_I}}\, M_{II} \sqrt{1 + \frac{\gamma_I - 1}{2} M_{II}^2} \ , \tag{D-19}$$

where

$\mathbb{R}_1$ = gas constant (lbf-ft/lbm-°R)

A_{1l} = exit flow area, equation (D-14) (L^2)

P_{1l} = exit pressure (lbf/L^2)

T_{ol} = stagnation temperature (°R)

g_c = 32.174 (lbm-ft/lbf-sec^2)

G_{Nl} = mass flow rate (lbm/sec)

If

$$F(M,\gamma) = M\sqrt{\gamma}\left[1 + \frac{\gamma - 1}{2} M^2\right]^{1/2} , \qquad \text{(D-20)}$$

then

$$G_{Nl} = P_{1l} A_{1l} \sqrt{\frac{g_c}{\mathbb{R}_1 T_{ol}}}\, F\left(M_{1l}, \gamma_1\right) . \qquad \text{(D-21)}$$

The function $F(M,\gamma)$ can be expressed in terms of M* as

$$F(M^*,\gamma) = \left[\frac{2\gamma}{\gamma + 1}\right]^{1/2} M^*\left[1 - \frac{\gamma - 1}{\gamma + 1} M^{*2}\right]^{-1} , \qquad \text{(D-22)}$$

or the nozzle mass flow rate becomes

$$G_{Nl} = P_{1l}\left[\frac{2\pi R_{1l}^2}{(1 + \cos\beta)}\right]\left[\frac{g_c}{\mathbb{R}_1 T_{ol}}\right]^{1/2} F(M^*,\gamma) . \qquad \text{(D-23)}$$

For uniform flow, $\beta = 0$, and conical flow $\beta > 0$.

5. The Quantity (ρU)

For an ideal gas,

$$\rho = \frac{P}{\mathbb{R}T} . \qquad \text{(D-24)}$$

then the mass flow rate per unit area is:

$$(\rho U) = \frac{p}{\mathbb{R}T} U = \frac{p}{\mathbb{R}T} \sqrt{2T_o C_p} \frac{U}{\sqrt{2T_o C_p}} . \qquad \text{(D-25)}$$

By definition of the Crocco number,

$$C \equiv U \Big/ \sqrt{2T_o C_p} = U/U_{max} . \qquad \text{(D-26)}$$

From the energy equation,

$$T + \frac{U^2}{2C_p} = T_o , \qquad \text{(D-27)}$$

the temperature ratio is found in terms of the Crocco number as

$$\frac{T_o}{T} = (1 - C^2)^{-1} . \qquad \text{(D-28)}$$

Rearranging equation (D-25) and substituting equation (D-26),

$$(\rho U) = \frac{p}{\sqrt{T_o}} \left[\frac{\sqrt{2C_p}}{\mathbb{R}}\right] \frac{T_o}{T} C , \qquad \text{(D-29)}$$

or combining equations (D-28) and (D-29),

$$(\rho U) = \frac{p}{\sqrt{T_o}} \left[\frac{\sqrt{2C_p}}{\mathbb{R}}\right] \frac{C}{(1 - C^2)} . \qquad \text{(D-30)}$$

But

$$C_p - C_v = \mathbb{R} \quad \text{or} \quad C_p = \frac{\gamma}{(\gamma - 1)} \mathbb{R}$$

$$(\rho U) = \frac{p}{\sqrt{\mathbb{R}T_o}} \left[\frac{2\gamma}{\gamma - 1}\right]^{1/2} \frac{C}{(1 - C^2)} . \qquad \text{(D-31)}$$

For $\mathbb{R}$ in units of (lbf-ft/lbm-°R), (ρU) is given by

$$(\rho U) = \frac{P}{\sqrt{\mathbb{R}T_o}} \left[\frac{2\gamma g_c}{\gamma - 1}\right]^{1/2} \frac{C}{(1 - C^2)} , \qquad \text{(D-32)}$$

where in equation (D-32)

ρ (lbm/ft^3)

U (ft/sec)

P (lbf/L^2)

T_o (°R)

$\mathbb{R}$ (lbf-ft/lbm-°R)

g_c (lbm-ft/lbf-sec^2)

6. Dimensionless Bleed Ratio, $\bar{B}$

The dimensionless bleed ratio [equation (D-8)] is

$$\bar{B} = \frac{-\left(G_E + G_I\right)}{G_{NI}} . \qquad \text{(D-8)}$$

By substitution of equations (D-1), (D-3), (D-23), and (D-32) into equation (D-8) and by using the condition that $P_{BE} = P_{BI} = P_B$, the result is

$$-\bar{B} = \frac{R_{imp}}{R_{1I}} \frac{P_B}{P_{1I}} \frac{\left(1 + \cos \beta_{1I}\right)}{F\left(M^*_{1I}, \gamma_I\right)} \frac{1}{\sigma_I} \frac{s_I}{R_{1I}} \sqrt{\frac{2\gamma_I}{\left(\gamma_I - 1\right)}} \left\{ C_{BI}\left[I_1\left(\eta_{dI}\right) - I_1\left(\eta_{jI}\right)\right] \right.$$

$$\left. + \frac{\sigma_I}{\sigma_E} \frac{S_E}{S_I} \left[\frac{\mathbb{R}_I}{\mathbb{R}_E} \frac{T_{oI}}{T_{oE}} \frac{\gamma_E}{\gamma_I} \frac{\left(\gamma_I - 1\right)}{\left(\gamma_E - 1\right)}\right]^{1/2} C_{BE}\left[I_1\left(\eta_{dE}\right) - I_1\left(\eta_{jE}\right)\right] \right\} \qquad \text{(D-33)}$$

7. Dimensionless Energy Ratio, $\bar{E}$

The dimensionless energy ratio [equation (D-13)] is

$$\bar{E} = -\left(E_E + E_I\right)/E_{NI} . \qquad \text{(D-13)}$$

By substitution of equations (D-21), (D-1), (D-10), (D-23), and (D-32) into equation (D-15) along with the conditions that

$$P_{BE} = P_{BI} = P_B$$

and

$$T_{BE} = T_{BI} = T_B$$

$$A_{BE} = T_B/T_{oE}$$

$$A_{BI} = T_B/T_{oI} \ ,$$

the dimensionless energy ratio is given by

$$-\bar{E} = \frac{R_{imp}}{R_{II}} \frac{\left(1 + \cos \beta_{II}\right)}{\sigma_I} \frac{s_I}{R_{II}} \frac{P_B}{P_{II}} \left[\frac{2\gamma_I}{\gamma_I - 1}\right]^{1/2} \left[F\left(M^*_{II}, \gamma_I\right)\right]^{-1}$$

$$\cdot \left\{ C_{BI} \left[I_3\left(\eta_{dI}\right) - A_{BI} I_1\left(\eta_{jI}\right)\right] + \frac{s_E}{s_I} \frac{\sigma_I}{\sigma_E} \left[\frac{\gamma_E}{\gamma_I} \frac{\left(\gamma_I - 1\right)}{\left(\gamma_E - 1\right)}\right]^{3/2} \left[\frac{R_E}{R_I} \frac{T_{oE}}{T_{oI}}\right]^{1/2} \right.$$

$$\left. C_{BE} \left[I_3\left(\eta_{dE}\right) - A_{BE} I_1\left(\eta_{jI}\right)\right] \right\} \qquad \text{(D-34)}$$

8. Coefficients: a_1, a_2, a_3

To simplify the notation of equations (D-33) and (D-34), the following coefficients have been defined. They are:

$$a_1 = \frac{R_{imp}}{R_{II}} \frac{\left(1 + \cos \beta_{II}\right)}{\sigma_I} \frac{s_I}{R_{II}} \frac{P_B}{P_{II}} \left[\frac{2\gamma_I}{\gamma_I - 1}\right]^{1/2} \left[F\left(M^*_{II}, \gamma_I\right)\right]^{-1} \qquad \text{(D-35)}$$

$$a_2 = \frac{s_E}{s_I} \frac{\sigma_I}{\sigma_E} \left[\frac{R_I}{R_E} \frac{T_{oI}}{T_{oE}} \frac{\gamma_E}{\gamma_I} \frac{\left(\gamma_I - 1\right)}{\left(\gamma_E - 1\right)}\right]^{1/2} \qquad \text{(D-36)}$$

$$a_3 = \frac{s_E}{s_I} \frac{\sigma_I}{\sigma_E} \left[\frac{\gamma_E}{\gamma_I} \frac{\left(\gamma_I - 1\right)}{\left(\gamma_E - 1\right)}\right]^{3/2} \left[\frac{R_E}{R_I} \frac{T_{oE}}{T_{oI}}\right]^{1/2} . \qquad \text{(D-37)}$$

3. Simplified Forms of $(\bar{B}, \bar{E})$

From equations (D-33), (D-35), and (D-36), the dimensionless mass bleed ratio becomes

$$-\bar{B} = a_1\left\{C_{B1}\left[I_1\left(\eta_{dI}\right) - I_1\left(\eta_{jI}\right)\right] + a_2 C_{BE}\left[I_1\left(\eta_{dE}\right) - I_1\left(\eta_{jE}\right)\right]\right\} \quad \text{(D-38)}$$

and from equations (D-34), (D-35), and (D-37), the dimensionless energy transfer ratio becomes

$$-\bar{E} = a_1\left\{C_{B1}\left[I_3\left(\eta_{dI}\right) - \Lambda_{B1} I_1\left(\eta_{jI}\right)\right] + a_3 C_{BE}\left[I_3\left(\eta_{dE}\right) - \Lambda_{BE} I_1\left(\eta_{jE}\right)\right]\right\} . \quad \text{(D-39)}$$

REFERENCES

1. Addy, A. L., Analysis of the Axisymmetric Base-Pressure and Base-Temperature Problem with Supersonic Interacting Freestream-Nozzle Flows Based on the Flow Model of Korst, et al., Part I: A Computer Program and Representative Results for Cylindrical Afterbodies, Report No. RD-TR-69-12, July 1969.

2. Addy, A. L., Analysis of the Axisymmetric Base-Pressure and Base-Temperature Problem with Supersonic Interacting Freestream-Nozzle Flows Based on the Flow Model of Korst, et al., Part III: A Computer Program and Representive Results for Cylindrical, Boattailed, or Flared Afterbodies, Report No. RD-TR-69-14, November 1969.

3. Shapiro, A. H., The Dynamics and Thermodynamics of Compressible Fluid Flow, I and II, Ronald Press, New York, 1953.

4. Ames Research Staff, Equations, Tables, and Charts for Compressible Flow, NACA Report No. 1135, 1953.

5. Hodgman, Charles D., Mathematical Tables from Handbook of Chemistry and Physics, Chemical Rubber Publishing Company, Cleveland, Ohio, 1947.

6. Addy, A. L., "The Analysis of Supersonic Ejector Systems," VKI LS-7, von Karman Institute for Fluid Dynamics, Brussels, Belgium, April 1968, pp. B-1 to B-156.

7. Love, E. S. Grigsby, C. E., Lee, L. P., and Woodling, M. J., Experimental and Theoretical Studies of Axisymmetric Free Jets, NASA Technical Report No. R-6, 1959.

8. Volkonskaya, T. B., "Calculation of Supersonic Axisymmetric Jets," A collection of papers of the Computational Center of the Moscow State University, Israel Program for Scientific Translations, Jerusalem, N66 26631, 1966.

9. Andrews, Earl H., Jr., Vick, Allen R., and Craidon, Charlotte B., Theoretical Boundaries and Internal Characteristics of Exhaust Plumes from Three Different Supersonic Nozzles, NASA Report No. TN D-2650, 1965.

REFERENCES (Concluded)

10. Callis, Linwood, B., An Analysis of Supersonic Flow Phenomena in Conical Nozzles by a Method of Characteristics, NASA Report No. TN D-3550, 1966.

11. Korst, H. H., "Compressible Two Dimensional Jet Mixing at Constant Pressure," University of Illinois, ME-TN-392-1, Office of Scientific Research TN-54-82 (reproduced as Office of Technical Services Collection, Pub. No. 132044, Dept. of Commerce), April 1954.

12. Page, R. H., and Korst, H. H., "Non-Isoenergetic Turbulent Compressible Jet Mixing with Consideration of Its Influence on the Base Pressure Problem," Proc. Midwestern Conf. Fluid Mech., 11, 1955, pp. 45-68.

13. Korst, H. H., Page, R. H., and Childs, M. E., "A Theory for Base Pressures in Transonic and Supersonic Flow," Univ. of Illinois, ME-TN-392-2, Office of Scientific Research TN-55-99, Contract No. AF 18 (600)-392, March 1955.

14. Korst, H. H., "A Theory for Base Pressures in Trasonic and Supersonic Flows," J. Appl. Mech., 23, 1956, pp. 593-600.

15. Korst, H. H., Chow, W. L., and Zumwalt, G. W., "Research on Transonic and Supersonic Flow of a Real Fluid at Abrupt Increases in Cross Section (with Special Consideration of Base Drag Problems)," Final Report, Univ. of Illinois, ME-TR-392-5, Office of Scientific Research TR-60-74, Contract No. AF 18 (600)-392, 1959.

16. Korst, H. H., "Turbulent Separated Flows," von Karman Institute for Fluid Dynamics, Course Note 66b, Rhode-Saint-Genese, Belgium, April 1967.

UNCLASSIFIED

Security Classification

DOCUMENT CONTROL DATA - R & D

(Security classification of title, body of abstract and indexing annotation must be entered when the overall report is classified)

1. ORIGINATING ACTIVITY (Corporate author)
Advanced Systems Laboratory
Research and Engineering Directorate (Provisional)
U. S. Army Missile Command
Redstone Arsenal, Alabama 35809

2a. REPORT SECURITY CLASSIFICATION
Unclassified

2b. GROUP
N/A

3. REPORT TITLE
DETAILED ANALYSES FOR THE BASE-PRESSURE PROGRAMS (TSABPP- 1,2)

4. DESCRIPTIVE NOTES (Type of report and inclusive dates)
Technical Note

5. AUTHOR(S) (First name, middle initial, last name)
A. L. Addy

6. REPORT DATE
25 August 1969

7a. TOTAL NO. OF PAGES
70

7b. NO. OF REFS
16

8a. CONTRACT OR GRANT NO

b. PROJECT NO (DA) 1M262301A206

c. AMC Management Structure Code No. 522C.11.118

d.

9a. ORIGINATOR'S REPORT NUMBER(S)
RD-TN-69-7

9b. OTHER REPORT NO(S) (Any other numbers that may be assigned this report)
AD

10. DISTRIBUTION STATEMENT
This document is subject to special export controls and each transmittal to foreign governments or foreign nationals may be made only with prior approval of this Command, ATTN: AMSMI-RD.

11. SUPPLEMENTARY NOTES
None

12. SPONSORING MILITARY ACTIVITY
Same as No. 1

13. ABSTRACT

The detailed development of the analyses which are the bases for the two-stream axisymmetric base-pressure programs (TSABPP-1,2) is presented. For the "corresponding" inviscid flow field, these analyses include the Prandtl-Meyer expansion, the oblique shock wave, the slip line, and the method of characteristics. For the turbulent-mixing component, two-dimensional constant-pressure mixing and its application to axisymmetric flows are considered.

DD FORM 1 NOV 68 1473 REPLACES DD FORM 1473, 1 JAN 68, WHICH IS OBSOLETE FOR ARMY USE.

UNCLASSIFIED
Security Classification

14. KEY WORDS	LINK A		LINK B		LINK C	
	ROLE	WT	ROLE	WT	ROLE	WT
Axisymmetric base-pressure programs						
Prandtl-Meyer expansion						
Oblique shock wave						
Slip line						